



NTNU – Trondheim
Norwegian University of
Science and Technology

Behaviour and Modelling of Fibre-Reinforced Polymers

Anne Helland Amundsen

Mechanical Engineering

Submission date: June 2014


Supervisor: Arild Holm Clausen, KT

Norwegian University of Science and Technology
Department of Structural Engineering



MASTER THESIS 2014

SUBJECT AREA: Polymer engineering	DATE: 10.06.2014	NO. OF PAGES: 14 + 72 + 17
--------------------------------------	---------------------	-------------------------------

TITLE: Behaviour and modelling of fibre-reinforced polymers Oppførsel og modellering av fiberarmerte plastmaterialer
BY: Anne Helland Amundsen


SUMMARY: This thesis evaluates the behaviour of polypropylene (PP) and glass fibre reinforced polypropylene with a glass fibre content of 10% and 30% by weight. Reinforcement materials are added to plastics to improve their mechanical properties and to reduce cost when compared to materials of similar strength. The difference in mechanical behaviour with increasing fibre content was examined using uniaxial tensile tests, bending tests and tensile tests on a plate with a centric hole. The application of fibre reinforced polymers have increased in the last years, and so has the need for a good material model. SIMLab at NTNU have created a material model used for ductile polymers and are now in the process of making a brittle polymer model. This model was tested on the 30wt% PP. The model was calibrated using the tensile tests and validated using the plate tests. The experimental tests showed that unreinforced polypropylene and glass fibre reinforced polypropylene are two different classes of materials. Whereas PP is ductile and isotropic, fibre reinforced PP is brittle and displays anisotropic behaviour. The material model was quite simple and included only anisotropic elasticity and brittle damage and fracture. This model worked well on the material in the longitudinal direction. In the 45 and 90 degree direction however it underestimated the maximum stress and strain. The material parameters in the material model were dependent on the material direction, and the damage parameters were not. The experimental tests showed that there were different fracture mechanisms in the different directions, and therefore the damage parameters should also be dependent on the material direction. The experimental tests on the plate with a centric hole revealed that the fibre reinforced material is also strain-rate dependent. This is something the material model does not take into account, and therefore, the material model either has to be calibrated at the same strain rate as it should be used, or the material model should take strain rate into account.
--

RESPONSIBLE TEACHER: Professor Arild H. Clausen
SUPERVISOR(S): Arild H. Clausen and Petter H. Holmstrøm
CARRIED OUT AT: SIMLab, Department of Structural Engineering, NTNU

SAMMENDRAG:

I denne oppgaven evalueres oppførselen til polypropylene (PP) og glassfiberarmert polypropylene med 10% og 30% glassfiberinnhold. Plast blir armert for å forbedre de mekaniske egenskapene til materialet og for å redusere kostnaden sammenlignet med materialer med lignende styrke. Forskjellen i mekaniske egenskaper med økende fiberinnhold ble undersøkt ved hjelp av strekktester, bøyetester og strekktester på plater med hull. Bruken av fiberarmerte plastmaterialer har økt de siste årene og det har også behovet for en god materialmodell. SIMLab ved NTNU har laget en materialmodell for duktile polymerer og er nå igang med å lage en materialmodell for sprø polymerer. Denne modellen ble testet på polypropylene med 30% glassfiber. Modellen ble kalibrert med strekktester og validert med plate med hull tester.

De eksperimentelle testene viste at polypropylene og glassfiberarmert polypropylene er to forskjellige klasser av materialer. PP er duktilt og isotropt mens fiberarmert PP er sprøtt og anisotropt.

Materialmodellen som ble brukt var ganske enkel og inkluderte bare anisotrop elastisitet of sprø skade og brudd. Modellen fungerte bra på materialet i lengderetningen, mens i 45 og 90 graders retning så undervurderte den maksimum spenning og tøyning. Materialparameterne i materialmodellen var avhengig av retningen på materialet, mens skadeparameterne var ikke det. De eksperimentelle testene viste at det var forskjellige bruddmekanismer i de forskjellige materialretningene, og derfor burde også bruddparameterne være avhengig av retning. De eksperimentelle testene på plate med hull viste også at det fiberarmerte materialet også var avhening av tøyningshastighet. Dette er noe materialmodellen ikke tar med, og derfor burde enten materialmodellen bli kalibrert med samme tøyningshastighet som den skal ha i bruk, eller så må materialmodellen også ta hensyn til tøyningshastighet.

MASTER THESIS 2014

Anne Helland Amundsen

Behavior and modelling of fibre-reinforced polymers

(Oppførsel og modellering av fiberarmerte plastmaterialer)

Polymers have low weight and excellent formability, and are therefore attractive materials for an increasing number of applications. However, the comparatively low stiffness and strength are a challenge. These properties can be substantially improved by introducing fibres during the production process. According to today's design practice, in particular in the automotive industry, all parts in a structure are normally modelled and analysed with the finite element method. To accurately predict the behaviour of the materials, the designers depend on reliable material models. For fibre-reinforced polymers, however, the models still need improvements.

The aim of this thesis is to study glass fibre-reinforced polypropylene with 0%, 10% and 30% fibre content. The materials are supposed to be characterized and existing material models should be applied to simulate the behaviour. Validation tests will be performed to validate the material models. It is of interest whether the material models are able to capture the observed response in the experimental tests.

Some keywords for activities related to this master thesis project may include:

- Literature survey: Properties of fibre-reinforced polymers and numerical aspects
- Experimental tests: Material tests, validation tests
- Material modelling: Adapt material models to include the effects seen in the experimental work. Determine material parameters.
- Numerical modelling: Simulation of experiments using Abaqus. Evaluation of material models.

The candidate may agree with the supervisors to pay particular attention to specific parts of the investigation, or include other aspects than those already mentioned.

The thesis is to be organized as a research report, recognizing the guidelines provided by Department of Structural Engineering.

Supervisors: Petter Henrik Holmstrøm and Arild Holm Clausen

The report is to be handed in not later than 11 June 2014.

NTNU, 20th January 2014

Arild Holm Clausen
Main supervisor

Acknowledgements

This thesis was written at the Structural Impact Laboratory at the Department of Structural Engineering at NTNU from January to June 2014.

Firstly, I would like to thank my main supervisor Professor Arild Holm Clausen, for outstanding guidance and support during the process of writing this thesis. A special thanks is directed to co-supervisor PhD student Petter Henrik Holmstrøm, for his invaluable contributions throughout the process. I would also like to thank Chief Engineer Trond Auestad for his support in the laboratory, Dr. Egil Fagerholt for his help with Digital Image Correlation and Dr. David Morin for support with the material model.

Anne Helland Amundsen

Trondheim, June 2014

Contents

Acknowledgements	i
Contents	v
List of Symbols	vii
Abbreviations	ix
1 Introduction	1
2 Theory	3
2.1 Polymers	3
2.1.1 Polypropylene	4
2.2 Composites	5
2.2.1 Matrix	5
2.2.2 Fibre	6
2.2.3 Glass Fibre-Reinforced Polypropylene	7
2.3 Injection Moulding	8
2.4 Introduction to the SIMLab Polymers Model	9
2.4.1 Anisotropic elastic materials	9
2.4.2 Brittle damage	12
3 Experimental Setup	15
3.1 Material	15
3.2 Experimental Programme	16
3.3 Uniaxial tension tests	18
3.4 Bending tests	19
3.5 Plate with centric hole	20
4 Experimental Results	23
4.1 Digital Image Correlation	23
4.2 Uniaxial tension tests	24
4.2.1 PP	27
4.2.2 PP10	29
4.2.3 PP30	30

4.2.4	Comparison and discussion	32
4.3	Bending tests	35
4.3.1	PP	36
4.3.2	PP10	37
4.3.3	PP30	38
4.3.4	Comparison and discussion	38
4.4	Plate with centric hole	41
4.4.1	PP	41
4.4.2	PP10	42
4.4.3	PP30	42
4.4.4	Comparison and discussion	43
4.5	Summary	45
5	Calibration	47
5.1	Parameters	47
5.1.1	Material parameters	48
5.1.2	Damage parameters	50
5.1.3	Parameters base model	51
5.2	Numerical model	52
5.2.1	Base model	53
5.3	Improvement of Material Parameters	54
5.3.1	Parametric study	54
5.3.2	Improved Model	58
5.4	Comparison and discussion	60
6	Validation	63
6.1	Plate with centric hole	63
6.1.1	Numerical model	63
6.1.2	Base Model	64
6.1.3	Improved model	65
6.2	Comparison and discussion	66
6.3	Evaluation of the SIMLab brittle polymers model	67
7	Conclusion	69
7.1	Further work	70
	Bibliography	71
	Appendices	I
	A Geometrical measurements	I
A.1	Experimental tests	II
	B Experimental Results	V
B.1	Uniaxial Tensile Tests	VI
B.2	Bending Tests	VIII

C	Abaqus input files	IX
C.1	Material cards	X
C.1.1	Base Material	X
C.1.2	Improved Material	X
C.2	Finite element analysis input files	XI
C.2.1	Tension test	XI
C.2.2	Plate with centric hole	XV

List of Symbols

$\dot{\epsilon}$	Strain rate
κ_0	Brittle damage threshold
κ_{0max}	Maximum value of κ_0
κ_{0min}	Minimum value of κ_0
κ_{0std}	Standard deviation of κ_0
ν	Poisson's ratio
σ	Stress
ϵ	Strain
G_f	Fracture energy
A	Cross-sectional area
E	Young's/Elastic modulus
F	Force
G	Shear modulus
L	Gauge length or span length
P	Load in bending tests
t	Thickness
v	Displacement
w	Width

Abbreviations

B test	Bending test
DIC	Digital Image Correlation
P test	Plate with centric hole test
PP	Polypropylene
PP10	Polypropylene with a 10% glass fibre content by weight
PP30	Polypropylene with a 30% glass fibre content by weight
SIMLab	Structural Impact Laboratory
T test	Tension test

Chapter 1

Introduction

The use of polymers has increased in the last decades due to their favourable properties such as easy formability, light weight, resistance to various chemicals and low cost. They are used in nearly all industries and especially in the structural and automotive industry. In some applications, materials which have the same formability and low weight as polymers, but higher strength and stiffness are needed. Fibre reinforced polymers can be an alternative. Fibre reinforced thermoplastic compounds may be processed by conventional methods, such as injection moulding, and offer improvements in mechanical properties.

Fibre reinforced polymers are a type of composite. Composites come in many forms, and is defined as a material made by combining two or more materials that are mutually insoluble by mixing or bonding in such a way that each maintains its integrity [1]. Composites have a wide range of uses, and their use is rapidly increasing. Man-made composites can be tailored to meet special needs such as high strength and stiffness combined with light weight. The resulting high-performance materials are increasingly being used in aircraft, space, and defence applications, and also in high grade sports equipment. A drawback to these materials is their high cost. More economical composites, such as glass-reinforced plastics, are continually finding new uses in a wide range of products, such as automotive components, boat hulls, sports equipment and furniture.

Glass fibre reinforced polypropylene moulding compounds have been available for many years. Since their initial development this class of materials has experienced a rapid growth in their end use applications. This can be attributed to the relative ease of processing combined with their clean and recyclable nature and an attractive price-performance ratio. However, as is typical with composite materials, there is a balance of processibility to performance. To obtain a high level of processibility with these moulding compounds, a certain level of the reinforcement efficiency of the fibres has to be given up [2].

According to today's design practice, in particular in the automotive industry,

all parts in a structure are normally modelled and analysed with the finite element method. Accurate material models are important to be able to predict the behaviour of the materials. Models for fibre reinforced polymers are quite new and still need improvements.

This thesis is written in cooperation with the Structural Impact Laboratory (SIM-Lab). SIMLab is a Centre for Research-based Innovation (SFI) located at the Department for Structural Engineering at the Norwegian University of Science and Technology (NTNU). One of SIMLab's research areas is dedicated to polymers and they have cooperated with several industries to improve the existing models of polymers. SIMLab has also developed a model for brittle polymeric materials such as fibre reinforced plastics. This model has not been tested near as much as the ductile polymeric models. This thesis will test this brittle polymer model on a glass fibre reinforced thermoplastic with 30 % fibre content by weight. The most important features included in the SIMLab brittle polymer is anisotropic elasticity and brittle damage and fracture.

Chapter 2

Theory

In this chapter the theoretical background most relevant for this thesis will be presented. Firstly, there will be a brief presentation of polymers and composites, before introducing polypropylene and glass fibre-reinforced polypropylene. The forming process of the plates used in the experiments will be presented as well as the brittle polymer model developed by SIMLab at NTNU.

2.1 Polymers

Polymers are materials consisting of long-chain molecules formed primarily by carbon-to-carbon bonds. The basic building blocks of the polymers are called monomers and these are generally repeated hundreds or thousands of times. Monomers can be linked in repeating units to make longer and larger molecules by a chemical reaction called polymerization. There are two important classes of polymerization:

1. In condensation polymerization, a stepwise reaction of molecules occurs and in each step a molecule of a simple compound, generally water, forms a by-product.
2. In addition polymerization, monomers join to form a polymer without producing any by-product. Addition polymerization is generally carried out in the presence of catalysts [3].

Polymers used as engineering materials can be classified into three groups: thermoplastics, thermosetting plastics, and elastomers. The difference between these groups is the polymerization process and bonding between the molecular chains. Thermoplastics are produced by addition polymerization and are characterized by linear chain molecules. They soften on heating and can be repeatedly melted or re-processed. Thermosetting plastics, however, changes chemically during processing. They undergo a curing reaction that involves cross-linking of the polymeric chains which makes them harden. Elastomers also experience cross-linking between the chains, however they occur less frequently than in thermosetting plastics, making the material more flexible. Linear molecules in thermoplastics result in higher

strain-to-failure values compared to those of thermosets. Thermoplastic materials can have failure strains ranging from 30 to 100 %, while the thermosets typically range from 1 to 3%. The large range of failure strains in thermoplastics stems from the rather large variation in the amount of crystallinity [4]. The density of the polymer chains defines amorphous and crystalline regions. In crystalline regions the chains are more tightly packed than in amorphous regions. A short bond is stronger than a long bond, which means that the crystalline regions are stronger than the amorphous regions. The difference between an amorphous and a semi-crystalline polymer structure is shown in Figure 2.1. Elastomers can be deformed by large amounts, say 100 to 200 % strain or more, with most of those deformation being recovered after removal of the stress [1]. Polypropylene is the material used in this thesis, and it is classified as a semi-crystalline thermoplastic.



Figure 2.1: Amorphous (left) and semi-crystalline (right) arrangement of polymer molecules.

On the basis of stress-strain behaviour, polymers fall within three general classifications: brittle, plastic and highly elastic. These materials are neither as strong nor as stiff as metals, and their mechanical properties are sensitive to changes in temperature and strain rate. However, their high flexibilities, low densities, and resistance to corrosion make them the materials of choice for many applications [5].

2.1.1 Polypropylene

Polypropylene is a semi-crystalline thermoplastic polymer. Some of the characteristics of polypropylene include resistance to heat distortion, excellent electrical properties and fatigue strength, as well as it being chemically inert and relatively inexpensive. It is often used in sterilizable bottles, packaging film, TV cabinets and luggage [5]. Figure 2.2 shows the polypropylene monomer on the left and the repeating unit on the right.

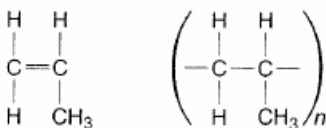


Figure 2.2: Monomer (left) and polymer repeating unit (right) of polypropylene [3].

Polypropylene is separated into three different categories: Homopolymer, consisting of only propylene based molecules. Random copolymer, a propylene-ethylene copolymer containing mainly propylene. And heterophasic copolymer, also referred to as high-impact PP or impact-modified PP.

2.2 Composites

Many of our modern technologies require materials with unusual combinations of properties that cannot be met by the conventional metals alloys, ceramics and polymeric materials. This is especially true for materials that are needed for aerospace, under-water, and transportation applications [5].

Composites are defined as a combination of two or more chemically distinct and insoluble phases whose properties and structural performance are superior to those of the constituents acting independently. Although plastics possess mechanical properties that are generally inferior to those of metals and alloys, these properties can be improved by embedding reinforcements of various types to produce reinforced plastics. Reinforcements improve the strength, stiffness, and creep resistance of plastics and particularly their strength-to-weight and stiffness-to-weight ratios [3].

Composite materials have a wide range of uses, and their use is rapidly increasing. Man-made composites can be tailored to meet special needs such as high strength and stiffness combined with light weight. The resulting high-performance (and expensive) materials are increasingly being used in aircraft, space and defence applications, and also for high-grade sports equipment, as in golf club shafts and fishing rods. More economical composites, such as glass-reinforced plastics, are continually finding new uses in a wide range of products, such as automotive components, boat hulls, sports equipment, and furniture [1].

Fibre reinforced composites consist of a matrix phase and a fibre phase. In this thesis, the polypropylene acts as the matrix and the glass fibre is the reinforcing fibre phase as the name suggests.

2.2.1 Matrix

The matrix phase of fibrous composites may be a metal, polymer, or ceramic. In general, metals and polymers are used as matrix materials because some ductility is desirable. For fibre-reinforced composites, the matrix phase serves three important functions:

1. Support and transfer the stresses to the fibres, which carry most of the load.
2. Protect the fibres against physical damage and the environment.
3. Reduce propagation of cracks in the composite by virtue of the ductility and toughness of the matrix [3].

It is essential that the adhesive bonding forces between fibre and matrix is high to minimize fibre pull-out.

2.2.2 Fibre

Reinforcements can be found in the form of particles, flakes, whiskers, short fibres, long fibres, continuous fibres or sheets. Most reinforcements used in composites have a fibrous form because materials are stronger and stiffer in the fibrous form than in any other form [4]. An important characteristic of most materials, especially brittle ones, is that a small diameter fibre is much stronger than the bulk material. The probability of a presence of a critical surface flaw that can lead to fracture diminishes with decreasing specimen volume, and this feature is used to advantage in the fibre reinforced composites. Glass fibre, in its various forms, have been the most common reinforcement for polymer matrices. Other examples of fibres used are aramid, carbon, boron and silicon carbide.

Fibres are frequently used as strengthening component because the load transfer from the matrix is especially effective if the strengthening phase is elongated in the loading direction. Furthermore, fibres may be advantageous because they are rather thin with a small diameter, which makes the defects in the material rather small [6].

The most important parameters affecting the mechanical properties of composite materials are fibre length and fibre content. The fibre content is determined depending on selected the selected matrix material, while the fibre length is determined depending on the geometry of the part to be produced. The main characteristics of the fibres that affect the effectiveness of the reinforcement are the diameter and length of the fibres and the fibre orientation and concentration.

Fibre size and length

The mechanical characteristics of a fibre-reinforced composite depend not only on the properties of the fibre, but also on the degree to which an applied load is transmitted to the matrix phase. Some critical fibre length is necessary for effective strengthening and stiffening of the composite material. This critical length l_c is dependent on the fibre diameter d and its ultimate strength σ_u , and on the fiber-matrix bond strength (or shear yield strength of the matrix, whichever is smaller) τ_c according to [5]

$$l_c = \frac{\sigma_u d}{2\tau_c} \quad (2.1)$$

If the fibre length is shorter than the critical value, the fibre is pulled out from its place due to the tension force and this results in poor mechanical properties. However, if the fibre length is longer than the critical value, the fibre is broken [7]. Fibres are classified as long or short. Long fibres are longer than the critical length and this means that the properties of the composite does not change when the fibre length is increased further. Short fibres are shorter than the critical length and a

change in the length has an influence on the properties of the composite [6]. Short fibres typically have an aspect ratio between 20 and 60, and long fibres between 200 and 500 [3]. Long fibres with an extension comparable to that of the whole component are frequently called continuous fibres.

The length of the fibres do not only determine the mechanical properties of the composite, but is also important for the manufacturing process as long fibres have to be processed differently than short fibres. Short fibres can be manufactured using the same processes used for the unreinforced matrix material [6].

Fibre orientation and concentration

Fibre arrangement is crucial relative to composite characteristics. The mechanical properties of continuous and aligned fibre composites are highly anisotropic. In the alignment direction, reinforcement and strength are a maximum; perpendicular to the alignment, they are a minimum. For short and discontinuous fibrous composites, the fibres may be either aligned or randomly oriented [5].

Glass Fibre

Glass fibres are the most widely used and least expensive of all fibres. Glass fibres are made by drawing molten glass through small openings in a platinum die and then mechanically elongated, cooled, and wound on a roll [3]. Glass is popular as a fibre reinforcement material for several reasons.

- It is easily drawn into high-strength fibres from the molten state.
- It is readily available and may be fabricated into glass-reinforced plastic economically using a wide variety of composite-manufacturing techniques.
- As a fibre it is relatively strong, and when embedded in a plastic matrix, it produces a composite having a very high specific strength.
- When coupled with the various plastics, it possesses a chemical inertness that renders the composite useful in a variety of corrosive environments [5]

2.2.3 Glass Fibre-Reinforced Polypropylene

In the case of glass-fibre reinforced polymers, the glass fibres increase the stiffness and strength, and the surrounding matrix makes the material more ductile and protects the fibres from concentrated loads. Glass fibre reinforced polypropylene moulding compounds have been available for many years. The glass fibre is the least expensive of all fibres and polypropylene is a thermoplastic which makes it cheaper and easier to process. These properties combined gives a composite which possess both higher performance and mass processibility.

2.3 Injection Moulding

Injection moulding is the most widely used technique for fabricating thermoplastic materials. This technique has been used to fabricate all the materials used in this thesis. An injection moulding machine with a plunger and reciprocating screw has been shown in Figure 2.3. The pellets, or granules, are fed into a heated chamber, where they are melted. The melt is then forced into a split-die chamber either by a hydraulic plunger or by the rotating screw of an extruder. Most modern equipment is of the reciprocating screw type [3]. The molten plastic is then injected into the mould cavity, where the pressure is maintained until the moulding has solidified. The most outstanding feature of this technique is the speed with which pieces may be produced, and because the material is molten when injected into the mould, complex shapes and good dimensional accuracy can be achieved. Another advantage is the low unit cost of injection moulded pieces. A main disadvantage is that the machine is very expensive. Injection moulded composites often contain relatively short fibres, shorter than the critical fibre length, oriented in complex and non-optimal patterns [2].

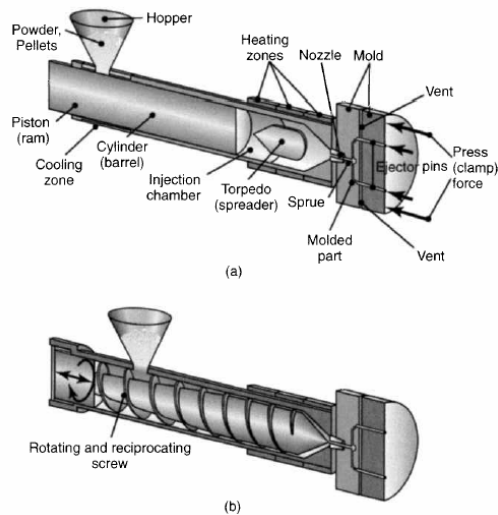


Figure 2.3: Injection moulding with (a) a plunger and (b) a reciprocating screw [3].

Fibre reinforced thermoplastics used in injection moulding are obtained by mixing polymer and fibres in an extruder and pelletizing. The fibre content is generally between 20 and 50 wt%, the fibre length is around $500 \mu\text{m}$, and the diameter is around $15 \mu\text{m}$. It is difficult to predict the actual fibre orientation in an injection moulded part. Most observations in injection moulded parts show two skin layers with preferential orientation parallel to the flow direction, and a core region with orientation perpendicular to the flow and in the plane of the part. In pure shear flow, fibres orient mainly in the flow direction, whereas in extensional flows, they orient in the direction of extension. Most injected parts have a nearly constant

thickness which is much lower than the other dimensions, therefore, shear deformations are dominant. The skin-core structure is more prominent in thicker parts with a thickness greater than 3 mm [8].

2.4 Introduction to the SIMLab Polymers Model

Material models for steel and aluminium have been developed and perfected for many years. That is not the case for polymers, and especially thermoplastics. SIMLab has been developing a material model for polymers for the past few years. The ductile polymer model used for thermoplastics has been tested and validated a number of times. SIMLab has also made a material model for brittle polymeric materials. This model is quite new and has not been tested properly. This thesis will apply this material model to a 30 wt% glass fibre reinforced thermoplastic.

The combined SIMLab polymers model accounts for isotropic/anisotropic elasticity, viscoelasticity, viscoplasticity, isotropic hardening and softening, molecular chain stretching (or kinematic hardening), pressure sensitivity, volume increase, brittle and ductile damage, and fracture. Isothermal conditions are assumed in order to limit the number of parameters. The model is developed for use with solid elements or shell elements [9].

The features included in the brittle model used for fibre-reinforced polymers are the anisotropic elasticity and the brittle damage and fracture. Viscoelasticity, viscoplasticity, isotropic hardening and softening, kinematic hardening, pressure sensitivity, volume increase and ductile damage is not included in this model [9]. This model is a very simple representation of a brittle material. This thesis will test this model and examine if the model is sufficient or if either it has to be changed or more features have to be added to be able to represent a fibre reinforced thermoplastic.

2.4.1 Anisotropic elastic materials

Real materials are never perfectly isotropic. In some cases, the differences in properties for different directions are so large that analysis assuming isotropic behaviour is no longer a reasonable approximation. Due to stiff fibres in particular directions, composite materials can be highly anisotropic, and engineering design and analysis for these materials requires the use of a more general version of Hooke's law. In the general three-dimensional case, there are six components of stress: σ_x , σ_y , σ_z , τ_{xy} , τ_{yz} and τ_{zx} , as illustrated in Figure 2.4. There are also six corresponding components of strain: ε_x , ε_y , ε_z , γ_{xy} , γ_{yz} , and γ_{zx} . In highly anisotropic materials, any component of stress can cause strain in all six components. The general anisotropic form of Hooke's law is given by the following six equations, here written with the coefficients shown as a matrix [1].

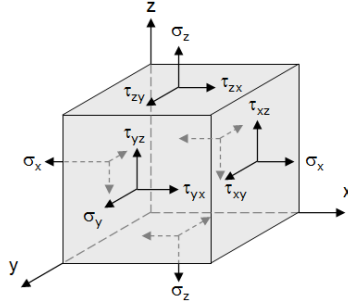


Figure 2.4: The six components needed to completely describe the state of stress at a point.

$$\begin{Bmatrix} \varepsilon_x \\ \varepsilon_y \\ \varepsilon_z \\ \tau_{yz} \\ \tau_{zx} \\ \tau_{xy} \end{Bmatrix} = \begin{bmatrix} S_{11} & S_{12} & S_{13} & S_{14} & S_{15} & S_{16} \\ S_{21} & S_{22} & S_{23} & S_{24} & S_{25} & S_{26} \\ S_{31} & S_{32} & S_{33} & S_{34} & S_{35} & S_{36} \\ S_{41} & S_{42} & S_{43} & S_{44} & S_{45} & S_{46} \\ S_{51} & S_{52} & S_{53} & S_{54} & S_{55} & S_{56} \\ S_{61} & S_{62} & S_{63} & S_{64} & S_{65} & S_{66} \end{bmatrix} \begin{Bmatrix} \sigma_x \\ \sigma_y \\ \sigma_z \\ \gamma_{yz} \\ \gamma_{zx} \\ \gamma_{xy} \end{Bmatrix} \quad (2.2)$$

$[S_{ij}]$ is called the compliance matrix. Materials having fibre structures and one distinct fibre direction may be orthotropic. Orthotropic materials have symmetry about three orthogonal planes. To deal with the situation of the S_{ij} values changing with the orientation of the x - y - z coordinate system, it is convenient to define the values for the directions parallel to the planes of symmetry in the material [1]. The SIMLab brittle polymer model assumes that the material exhibits orthotropic symmetry and that the coordinate axes are along the symmetry axes of the material [9]. In this particular coordinate system, shear stresses will not produce normal strains and vice versa.

$$[S_{ij}] = \begin{bmatrix} \frac{1}{E_X} & -\frac{\nu_{YX}}{E_Y} & -\frac{\nu_{ZX}}{E_Z} & 0 & 0 & 0 \\ \frac{\nu_{XY}}{E_X} & \frac{1}{E_Y} & -\frac{\nu_{ZY}}{E_Z} & 0 & 0 & 0 \\ \frac{\nu_{XZ}}{E_X} & -\frac{\nu_{YX}}{E_Y} & \frac{1}{E_Z} & 0 & 0 & 0 \\ 0 & 0 & 0 & \frac{1}{G_{YZ}} & 0 & 0 \\ 0 & 0 & 0 & 0 & \frac{1}{G_{ZX}} & 0 \\ 0 & 0 & 0 & 0 & 0 & \frac{1}{G_{XY}} \end{bmatrix} \quad (2.3)$$

In Equation (2.3), there are three Young's moduli E_X , E_Y , and E_Z for the three different material directions. There are also three different shear moduli G_{XY} ,

G_{YZ} , and G_{ZX} corresponding to three planes. The constants ν_{ij} are the Poisson's ratios:

$$\nu_{ij} = -\frac{\varepsilon_j}{\varepsilon_i} \quad (2.4)$$

Because of the symmetry of S_{ij} values about the matrix diagonal,

$$\frac{\nu_{ij}}{E_i} = \frac{\nu_{ji}}{E_j} \quad (2.5)$$

where $i \neq j$ and $j = X, Y,$ or Z . These relationships reduces the number of independent Poisson's ratios to three for a total of nine independent constants [1]. The SIMLab polymer model uses these nine constants to describe the anisotropic nature of the brittle polymeric material [9].

A special case of the orthotropic material is the transversely isotropic material, where the properties are the same for all directions in a plane, such as the Y-Z plane, but different for the third (X) direction. Here there are five independent elastic constants as $E_Y = E_Z$, $\nu_{XY} = \nu_{ZX}$, $G_{XY} = G_{ZX}$ and the shear modulus G_{YZ} can be found from E_Y and ν_{YZ} using the relationship in Equation 2.6.

$$G_{YZ} = \frac{E_Y}{2(1 + \nu_{YZ})} \quad (2.6)$$

This simplification can often be used for fibre reinforced composites where all the fibres are in parallel and have a circular cross-section. In a unidirectional composite, the plane normal to the fibre direction can be considered the isotropic plane.

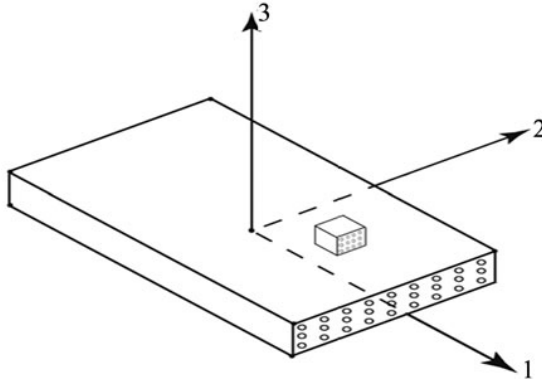


Figure 2.5: Arrangement of fibre direction for transversely isotropic composite.

Figure 2.5 shows a unidirectional composite where the 1-axis is aligned with the fibre direction, the 2-axis is in the plane of the layer and perpendicular to the fibres, and the 3-axis is perpendicular to the plane of the layer and thus also perpendicular to the fibres. Here the 2-3 plane is the isotropic plane.

2.4.2 Brittle damage

Fibre reinforced materials are usually brittle materials, and therefore a brittle damage evolution rule should be defined. The theory behind the brittle damage rule is taken from the theory manual made for the SIMLab polymers model [9]. In brittle materials, fracture is often initiated because of defects in the material and since not all fibres fail simultaneously, a statistical distribution of the damage parameters are needed.

An equivalent deformation measure $\bar{\varepsilon}_D$ is defined as

$$\bar{\varepsilon}_D = \sqrt[a]{\sum_{i=1}^3 \langle \hat{\varepsilon}_i \rangle^a} \quad (2.7)$$

where $\hat{\varepsilon}_i$ ($i = 1,2,3$) are the principal values of a rotationless deformation tensor:

$$\hat{\varepsilon}(t) = \int_0^t \hat{D} dt \quad (2.8)$$

where t is the time.

The loading/unloading conditions for damage are expressed in Kuhn-Tucker form as

$$f_D = \bar{\varepsilon}_D - \kappa \leq 0, \quad \dot{\kappa} \geq 0, \quad \dot{\kappa} f_D = 0 \quad (2.9)$$

A damage threshold can be introduced by giving κ a positive initial value κ_0 , i.e. for $\kappa \leq \kappa_0$ there is no damage evolution. κ equals the maximum value of $\bar{\varepsilon}_D$ reached during the straining history, and the damage only grows when the critical state is exceeded. The damage evolution law is then formulated as

$$D(\bar{\varepsilon}_D) = 1 - \frac{\kappa_0}{\kappa_1 - \kappa_0} \left(\frac{\kappa_1}{\bar{\varepsilon}_D} - 1 \right) \quad (2.10)$$

where κ_1 is a parameter shown in Figure 2.6. In a uniaxial tensile test, the longitudinal strain ε is equal to both $\bar{\varepsilon}_D$ and κ . If E_0 is the elastic modulus of the material. Then, the behaviour described by the elastic-damage model in the tensile test is illustrated in Figure 2.6.

The shaded area under the stress-strain curve is the amount of energy dissipated within a cubical finite element with characteristic length h_e , at failure. The energy dissipation due to damage should be invariant of element size, therefore the fracture energy G_f is defined as:

$$G_f A_e = \frac{1}{2} E_0 \kappa_0 \kappa_1 V_e \quad (2.11)$$

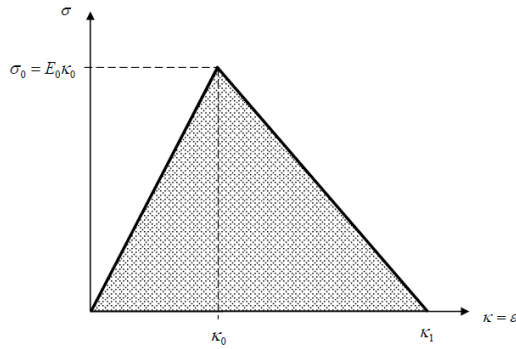


Figure 2.6: Stress-strain curve for a single element in uniaxial tension in the reference direction.

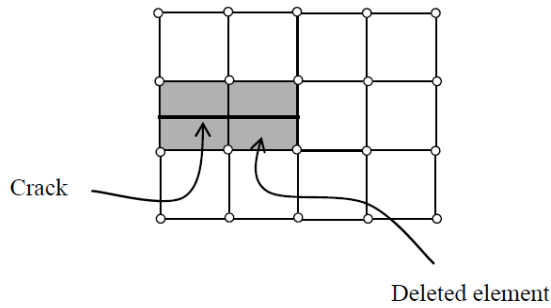


Figure 2.7: Crack propagation by erosion of elements.

Fracture - element erosion

Fracture and crack propagation are described by element erosion. As one or several of the fracture criteria applied are reached in an integration point, the stress tensor is set to zero, and this integration point can no longer carry load. If a user-defined number of integration points of a finite element has failed, then the element is eroded, which implies that the element has no residual load-carrying capacity and gives no contribution to the internal forces.

Statistical distribution

For brittle materials it may be necessary to distribute the fracture parameters to account for the defect distribution of the material. The fracture parameter κ_0 can be assumed to be a stochastic variable defined either by a Weibull distribution or a normal distribution. As the normal distribution is the one applied in this thesis,

the Weibull distribution will not be explained further. Figure 2.8 shows a normal distributed curve with standard deviation.

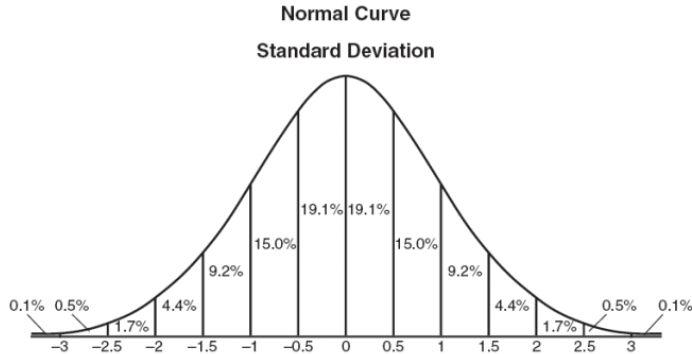


Figure 2.8: Normal distribution curve with standard deviation.

The normal distribution is a statistical distribution defined by a mean value, in this case, $\bar{\kappa}_0$ and a standard deviation of κ_0 , κ_{0std} .

$$f(\kappa_0) = \frac{1}{\kappa_{0std}\sqrt{2\pi}} \exp \left[-\frac{1}{2} \left(\frac{\kappa_0 - \bar{\kappa}_0}{\kappa_{0std}} \right)^2 \right] \quad (2.12)$$

To avoid unrealistically small or large values of the stochastic variable κ_0 , the distributions can be truncated by the user. The allowable range of κ_0 is then defined as

$$0 < \kappa_{0min} \leq \kappa_0 \leq \kappa_{0max} \quad (2.13)$$

here the maximum and minimum values $\kappa_{0min} \geq 0$ and $\kappa_{0max} > 0$ are user-defined.

Without statistical distribution all elements would fail at the same time creating a linear graph.

Chapter 3

Experimental Setup

In this chapter the experimental setup is presented. A total of 54 experimental tests were performed. This included 27 uniaxial tension tests, 18 bending tests and 9 tension tests on a plate with a centric hole. The tests were performed in order to examine and compare the materials and to calibrate and validate the brittle polymer material model.

3.1 Material

The materials studied in this thesis were unreinforced polypropylene (PP), PP with a glass fibre content of 10% by weight (PP10) and PP with a glass fibre content of 30% (PP30). The materials were left over materials from a PhD thesis by Andreas Koukal done for Audi and had been stored at NTNU in suboptimal conditions, i.e. in an office at room temperature. All three materials have been injection moulded. The materials studied were SABIC PP 579S for the unreinforced PP, SABIC STAMAX 30YM240 for the 30% fibre reinforced PP and a mix of the two previous materials for PP10.

The material properties found from the data sheets supplied by SABIC are shown in Tables 3.1 and 3.2. There were no available data for the 10% glass fibre material, since this material was exclusively made for Koukal's PhD project. We can assume that the properties for this material will lie somewhere between those of the unreinforced PP and PP30, though most likely closer to PP30.

The supplier describes the PP 579S material as having been specifically developed for use in thin-walled antistatic containers. The material has outstanding flow properties and a high stiffness, enabling high production rates. Special characteristics are low tendency for warpage, high lot to lot consistency, good contact transparency and high gloss. It is a made with a homopolymer polypropylene.

Table 3.1: Typical values for the material properties of SABIC PP 579S [10].

Properties	Value	Units	Test Methods
Density	905	kg/m ³	ISO 1183
Stress at yield ¹⁾	36	MPa	ISO 527-2 1A
Strain at yield ¹⁾	9	%	ISO 527-2 1AB
Tensile Modulus ²⁾	1750	MPa	ISO 527-2 1A

1) Speed of testing 50 mm/min

2) Speed of testing 1 mm/min

SABIC describes the STAMAX 30YM240 material as a 30% long glass fibre reinforced polypropylene developed to be injection moulded for the automotive industry. The glass fibres are chemically coupled to the PP matrix, resulting in high stiffness and strength.

Table 3.2: Typical values for the material properties of SABIC STAMAX 30YM240 [11].

Properties	Value	Units	Test Methods
Glass fibre content	30	%	ISO 3451
Density	1120	kg/m ³	ISO 1183
Tensile Strength	110	MPa	ISO 527/1B
Tensile elongation at break	2.3	%	ISO 527/1B
Tensile Modulus	6650	MPa	ISO 527/1B

SABIC describes the material as a long glass fibre material, however, it is not known how long the fibres are nor the size of them. The exact orientation of the fibres is also unknown, however we assume that they lie more or less along the longitudinal direction of the plates. The materials were delivered in 2010 as injection moulded plates with nominal thickness of about 2.7 mm.

3.2 Experimental Programme

The tension tests were performed in 3 material directions, the bending test in 2 and the plate tests were performed in one material direction. All tests were performed with three repetitions to ensure repeatability. The tests were performed under quasi-static loading conditions in room temperature. An overview of the experimental program can be found in table 3.3.

Table 3.3: An overview of the experimental program. All tests were performed for all three materials.

Test type	Material Orientation	Repetitions	Date, 2014
Uniaxial tension (T)	0, 45, 90	3	05.-07.02
Bending (B)	0, 90	3	17.-18.03
Plate with hole (P)	0	3	05.-07.02

The specimens were machined from two different rectangular plates for each material into the geometries shown in Figures 3.2, 3.4, and 3.6. The tests in the 0 degree direction were machined from the longitudinal direction of the injection moulded plates, and the tests in the 90 degree direction were taken from the transversal direction. The 45 degree specimens were taken out 45 degrees to the longitudinal direction. Since the plates were only approximately 2.7 mm thick they were used with their original thickness.

The name system assigned in the tests follows the syntax X-PPYY-ZZ-N. X refers to the test type (T = tension, B = bending and P = plate with hole), YY indicates the fibre content, ZZ is the angle between the longitudinal direction of the specimen and the direction of the moulded material, and N refers to the repetition number. As an example T-PP10-45-2 is the second uniaxial tension test in the 45 degree direction.

All test specimens were painted with a black and white speckled pattern to be able to use digital image correlation (DIC) in the post-processing of the results. A painted tensile specimen can be seen in Figure 3.1.

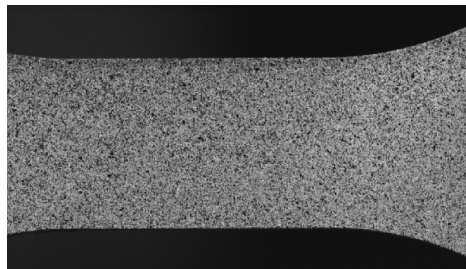


Figure 3.1: Speckle pattern on tensile specimen.

The speckled pattern consists of an undercoat of white spray paint randomly speckled with black paint. To ensure that the paint would not become dry and crack up during the test, the paint was applied shortly before testing. The camera rig then photographed the specimens at a rate adapted to the strain rate and length of testing. The pattern created by the two layers of paint could then be read by an image correlation program, in this case a program named eCorr created by SIMLab at NTNU. The program puts the pictures in succession, sorted by name.

Then the user places a mesh on the images to mark the area from where information should be gathered. The program then uses the speckled pattern to correlate the physical deformation with the deformation shown in the pictures. Since fibre-reinforced polymers are brittle, the strains experienced by the test specimens will be smaller than those of unreinforced polymers and metals. These small strains can be challenging to capture using regular DIC. To counteract this, the speckled pattern used in the tests were smaller than patterns used previously. Because of the small pattern, a new zoom lens able to capture this pattern had to be used, as well as a higher picture rate. Section 4.1 will give a more thorough introduction to digital image correlation.

3.3 Uniaxial tension tests

Quasi-static uniaxial tension tests were performed on all three materials. Strain rates of $\dot{\epsilon}_{nom} = 10^{-3}\text{s}^{-1}$ ensured the tests to be quasi-static.

The geometry of the tension specimens is shown in Figure 3.2 and pictures from the experiments are found in Figure 3.3. The nominal length of the primary deformation area was 15 mm, the nominal width was 10 mm and the overall nominal length of the specimens was 100 mm. The nominal thickness of the specimen was about 2.7 mm. The exact dimensions of the thickness and width in the primary deformation area were measured at two places along the length, identified by the coloured lines in Figure 3.2. The average values of the two measurements were used in the computation of engineering stress. The geometry measurements before testing can be found in Table A.1.

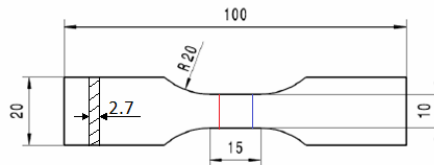


Figure 3.2: Nominal geometry of the tensile test specimens.

The tests were performed using a Zwick/Roell Z030 30kN universal test machine. The test specimens were painted in the black and white speckled pattern, as described previously, on the front and side of the test specimen. Two high speed cameras were set up, with the eCorr DIC software, to log images of the front and side during loading. The images were logged together with a log file from the cross-head giving the time, force and displacement from the machine. The logging frequency was 0.5 Hz for PP and 3 Hz for PP10 and PP30. The test setup with the cameras can be seen in Figure 3.3 (a) and the specimen mounted in the machine can be seen in Figure 3.3 (b).

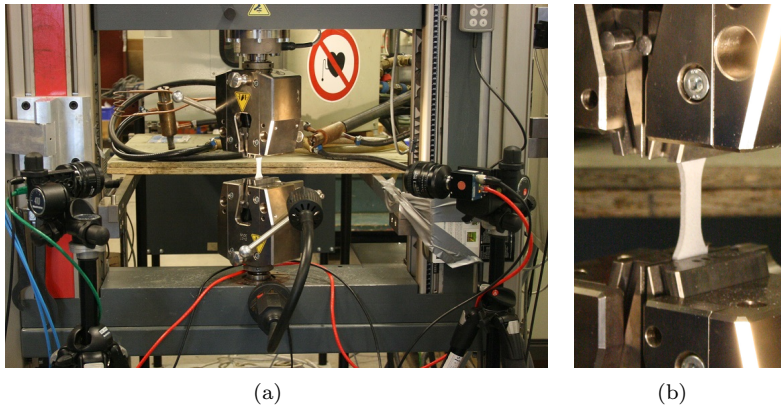


Figure 3.3: (a) Overview of test setup for quasi-static tests and (b) uniaxial tensile specimen mounted in the loading machine.

All tension tests were performed with a cross-head velocity of 0.9 mm/min, which corresponds to a nominal strain rate of approximately $\dot{\epsilon}_{nom} = 10^{-3}\text{s}^{-1}$.

3.4 Bending tests

The geometry of the bending specimen is shown in Figure 3.4. The nominal length of the specimen was 60 mm, the nominal width was 30 mm and the nominal thickness was 2.7 mm. The length was measured at two locations, the width at three locations and the thickness at three locations. The average measurements were used in the post-processing of the results. The measurement locations is shown in Figure A.2 and the geometry measurements before testing can be found in Table A.2. The width of the specimen was chosen to be able to ensure plane strain conditions.

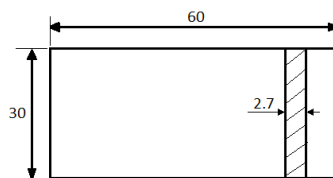


Figure 3.4: Nominal geometry of the bending test specimens.

The tests were performed using a Zwick/Roell Z030 30kN universal test machine. The specimens were painted with a black and white speckled pattern on the side and a high speed camera was set up to log pictures during the test, as can be seen in Figure 3.5 (a). The DIC logging frequency was 10Hz. A close-up of the bending specimen mounted in the loading machine is shown in Figure 3.5 (b).

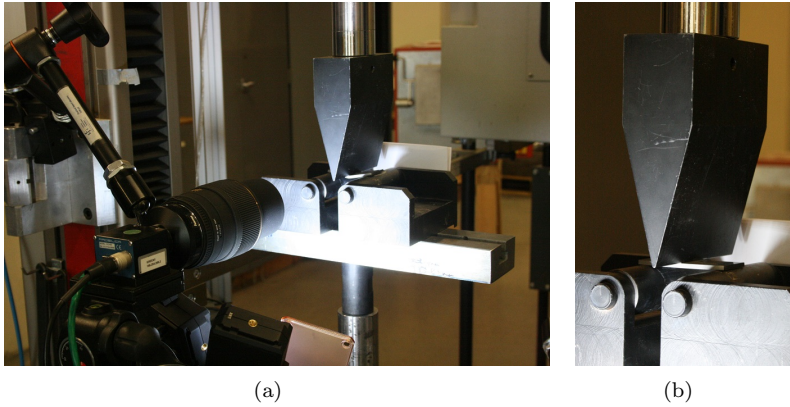


Figure 3.5: (a) Overview of test setup for quasi-static bending tests and (b) bending specimen mounted in the loading machine.

The wedge tip impacting the plate had a diameter of 2.5 mm and the span length was 50.7 mm. The bending tests were performed with a cross-head velocity of 9 mm/min giving an approximate nominal strain rate of $\dot{\epsilon}_{nom} = 10^{-3}\text{s}^{-1}$, with small variations depending on the strength of the material.

3.5 Plate with centric hole

The geometry of the plate is shown in Figure 3.6. The nominal dimensions of the plate is 100 mm length and 30 mm width with a 15 mm in diameter hole in the centre. The nominal thickness was approximately 2.7 mm. The width of the plate at the center and the width and thickness at each side of the hole was measured before the test. The geometry measurements can be found in Table A.3, and Figure A.3 shows where the measurements were taken.

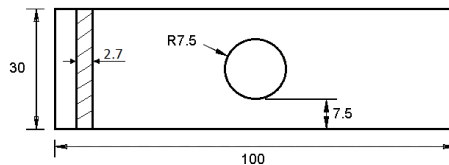


Figure 3.6: Nominal geometry of the component test specimens.

The plate was mounted in the Zwick/Roell Z030 loading machine in the same manner as the uniaxial tensile tests. The specimens were painted with the black and white pattern at the front and a high speed camera was used to log pictures during the test. The logging frequency changed slightly for each test. This was because the frequency was overestimated at the beginning and gave more frames

than was necessary. An overview of the logging frequency for each test is shown in Table 3.4.

Table 3.4: DIC logging frequency for all tests on plate with a centric hole.

Log frequency [Hz]			
	Repetition		
Material	1	2	3
PP	0.5	1	5
PP10	5	3	7
PP30	3	2	7

The test specimen mounted in the machine can be seen in Figure 3.7.

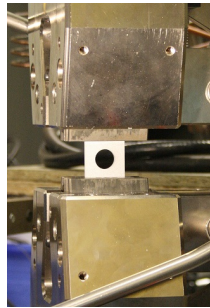


Figure 3.7: Plate with hole mounted in loading machine.

All the tests were supposed to be performed with the same cross-head velocity of 0.18 mm/min, which would correspond to an approximate nominal strain rate of $\dot{\epsilon}_{nom} = 10^{-3}\text{s}^{-1}$. This however is proven to be wrong after looking at the test results. The first and second repetitions for each material is found to have been tested at a strain rate of approximately $\dot{\epsilon}_{nom} = 10^{-4}\text{s}^{-1}$, while the third repetitions were tested at a strain rate of approximately $\dot{\epsilon}_{nom} = 10^{-3}\text{s}^{-1}$. This is explained further in the experimental results of the plate with a centric hole.

Chapter 4

Experimental Results

In this chapter the experimental results from the previous chapter will be presented. The tests were post processed using digital image correlation and Matlab. First there will be an introduction to post processing using DIC, then the results will be presented and discussed.

4.1 Digital Image Correlation

In addition to traditional extensometry, optical strain measurement devices have been increasingly applied in recent years for various materials to characterize their mechanical behaviour. In contrast to clip-on or contact extensometers, which are mechanically attached to the test specimen, optical measurement devices operate contactless. Optical techniques are particularly suitable for soft polymeric materials, as local stress concentrations arising from the indentation of the specimen and the weight of an attached mechanical extensometer are entirely avoided. Using optical extensometry can be favourable for fibre-reinforced polymers as well as these have very small strains that a mechanical device can have trouble to pick up. There are in principal two optical strain measurement systems that can be distinguished. These are devices with a fixed gauge length measuring the strain between two marks on the test specimen, i.e. optical extensometers, and full-field strain analysis referred to as digital image correlation [12].

In general, DIC is based on the principle of comparing speckle pattern structures on the surface of the deformed and the undeformed sample or between any two deformation states. The user places a mesh on the speckled pattern of the specimen and runs an analysis to correlate the pattern within each element of the mesh frame by frame. The information wanted can then be extracted. The longitudinal and transverse strains in the plane can be extracted without assuming the constitutive behaviour of the material a priori and strains can also be extracted after necking. To extract information, the user can either select elements to get the true strains for that element directly, or select a node or vector to get displacement

or elongation respectively. When combining the strain information from the DIC with the force logged by the machine, force-displacement or stress-strain curves can be made. The information wanted in each test was extracted in a text file and imported into Matlab for further post-processing. Further information on the information extracted can be found in their respective sections.

As mentioned in the previous chapter, the strains measured in this thesis is much smaller than strains usually measured with DIC. For traditional extensometry, the limits of resolution and accuracy are well known and can easily be determined. In the case of optical measurement devices the situation is more complicated, since resolution and accuracy depend on the whole measurement system including the objective, the camera and the light system [12]. The speckled pattern applied to the specimens were much smaller than speckle pattern previously used, and a zoom lens capable of higher resolution was used to be able to detect the new pattern. It seemed like this was sufficient, and the results portrayed the material correctly. There is some uncertainty in the method as increasing the resolution too much can make it reach a point where the error in the method is in the same order of magnitude as the phenomenon that is measured.

4.2 Uniaxial tension tests

The results in this section will be presented with true stress-strain curves. The strains were found using the DIC software eCorr as described above. For the unreinforced PP, the average strains over the elements in the necking region was used to get the true strains directly, as shown in Figure 4.1. Both the strains in the longitudinal and transverse direction could be found from these elements. The strains in the thickness direction had to be found using DIC on the side of the test specimen in the same way. A reason for using the mean strain in the necking region is to reduce the numerical noise that occur in the correlation process.

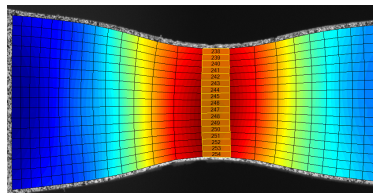


Figure 4.1: Direct strain from DIC using the average of the strains in the necking region from PP.

The glass fibre reinforced polymers did not experience necking, therefore this method could not be used. The strain field from the reinforced materials can be seen in Figure 4.2. This shows that there is no highly strained neck region as in PP in Figure 4.1. The strain is distributed inhomogeneously in the specimen, and it is not known if this effect is the real strain pattern or an effect created from numerical noise. It was therefore decided to use vectors in the length, width and

thickness directions instead of element strains. This would work similar to an optical extensometer. The results from the vectors was tested against the average of the strains in the middle elements along the length, and it was found to give very similar results.

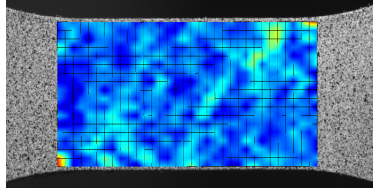


Figure 4.2: Strain field on PP30

The average of 5 vectors in the longitudinal direction and 10 in the width and thickness directions were used to get the respective strains. Figure 4.3 shows the vectors in the length and width directions, and the vectors in the thickness direction were applied in the same manner.

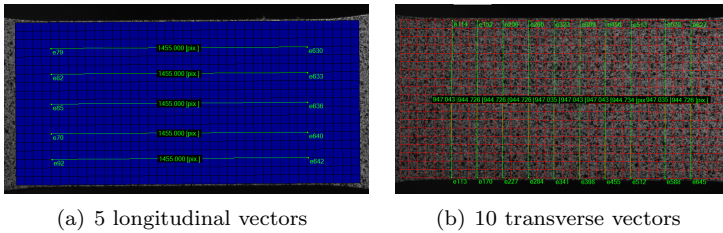


Figure 4.3: Vectors applied in the longitudinal and transverse direction.

The strains obtained from this method were engineering strains, $\varepsilon_{eng} = \Delta L/L_0$ for the longitudinal direction, with the same relationship in the width and thickness directions. This had to be converted into true (or logarithmic) strain and the following formula was used:

$$\varepsilon_{true} = \ln(1 + \varepsilon_{eng}) \quad (4.1)$$

During testing, the force, cross-head displacement and time were measured by the testing machine and logged together with the images captured with the DIC software. The true stress can be found by dividing the force F by the cross-sectional area A at any time during the test.

$$\sigma_{true} = \frac{F}{A} \quad (4.2)$$

The change in area during the test is difficult to measure, therefore the initial cross-sectional area A_0 is used to get the engineering stress

$$\sigma_{eng} = \frac{F}{A_0} \quad (4.3)$$

Since the DIC was applied on both the front and the side of the specimen, it is possible to extract the strains in the width and thickness directions, as well as the longitudinal direction. The true strains in each direction is shown in Equation (4.4).

$$\varepsilon_l = \ln \frac{l}{l_0} \quad \varepsilon_w = \ln \frac{w}{w_0} \quad \varepsilon_t = \ln \frac{t}{t_0} \quad (4.4)$$

Where l , w and t is the gauge length, width and thickness respectively at any time during the test, and l_0 , w_0 , and t_0 is the initial length width and thickness of the specimen respectively. The cross-sectional area of the specimen is $A = wt$. Putting the exponent in front of ε_w and ε_t and rearranging gives:

$$w = w_0 e^{\varepsilon_w} \quad \text{and} \quad t = t_0 e^{\varepsilon_t} \quad (4.5)$$

which inserted in the area gives:

$$A = w_0 t_0 e^{\varepsilon_w} e^{\varepsilon_t} = A_0 e^{\varepsilon_w} e^{\varepsilon_t} \quad (4.6)$$

Inserting Equation 4.6 into Equation 4.2 gives the true stress expressed as a function of the engineering stress and the true strains in the width and thickness.

$$\sigma_{true} = \frac{F}{A_0} e^{-\varepsilon_w} e^{-\varepsilon_t} = \sigma_{eng} e^{-\varepsilon_w} e^{-\varepsilon_t} \quad (4.7)$$

If the strains in the width and thickness directions are equal, or close to equal, $\varepsilon_w \approx \varepsilon_t$, this is often simplified using only the transverse strain ε_w , since it is easier to only measure ε_w .

$$\sigma_{true} = \sigma_{eng} e^{-2\varepsilon_w} \quad (4.8)$$

In some materials it is acceptable to assume the volume is constant during testing. This gives a new simplified true stress measure:

$$\sigma_{true} = \sigma_{eng} (1 + \varepsilon_{eng}) \quad (4.9)$$

Before the final true stress-true strain curves were made, a representative test from each material quality was chosen to investigate which method of obtaining the true stress was sufficient. Polypropylene is a polymer and these materials are known to experience volume change during tensile testing. This could also be seen in this material, and therefore Equation (4.9) could not be used. The strains in the thickness and width directions were not found to be equal, they were similar however, and because of voids forming on the side of the specimens during testing making it difficult to get ε_t from DIC, it was decided to use Equation (4.8) to get the true stress for PP.

PP10 and PP30 were found to be brittle materials and did not seem to have any significant change in volume during testing. The three methods for obtaining true stress yielded very similar results and it was therefore decided to use the simplest method from Equation (4.9).

4.2.1 PP

The resulting true stress-strain curves from the tensile tests on the unreinforced PP can be seen in Figure 4.4.

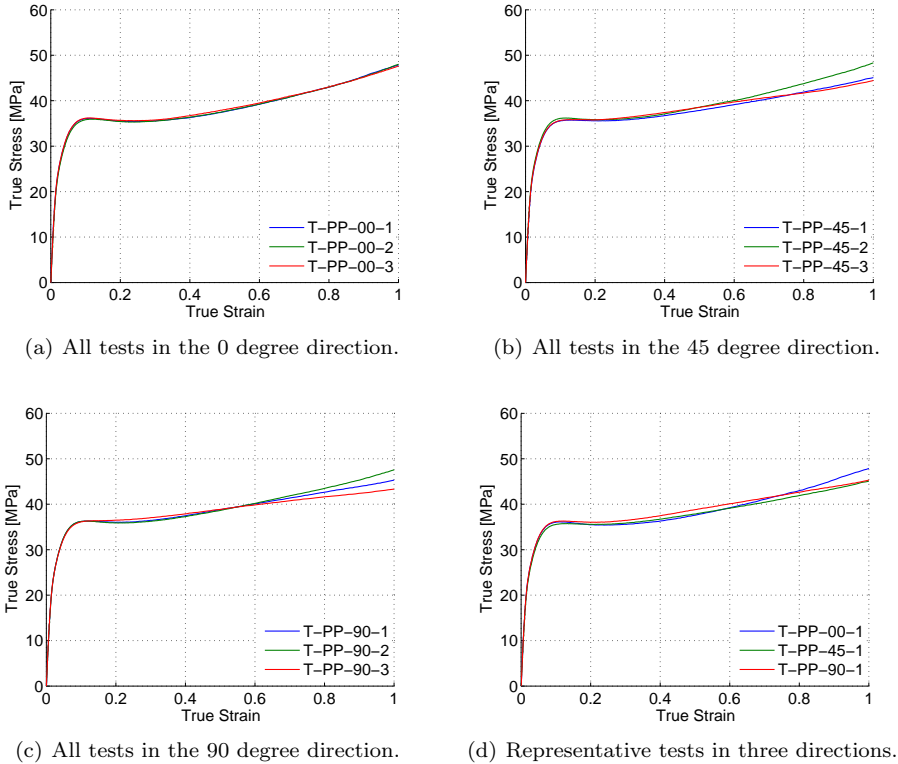


Figure 4.4: True stress-true strain curves for the PP tension tests.

Figure 4.4 (a), (b) and (c) shows the curves in the 0, 45 and 90 degree directions respectively and (d) shows the tests chosen to represent each material direction. The stress-strain curves of the unreinforced PP only shows the strain up to 1 as higher strains are not relevant to this study, and the graphs presented show the stress-strain relationship typical for polymers. The tests were stopped after a cross-head displacement of 30 mm, before fracture occurred. The tests show that PP is relatively isotropic as the tests in the different directions does not differ substantially. The variations in the three directions are not larger than the variations in the three repetitions of each test. Polypropylene has a low load capacity and high ductility compared to most other engineering materials. It is seen that the material slightly softens before hardening is initiated. All tests have a yield stress of approximately 36 MPa at about 10 % strain. Both the yield stress and strain is taken at the initial stress peak in the true stress-strain curves. The

data sheet given by SABIC in Table 3.1 gives a stress at yield of 36 MPa and a strain at yield of 9 %. This corresponds well to the values found in the experiments. The average elastic modulus found for PP is 1508 MPa for all three directions and this lower than the manufacturer's value of 1750 Mpa.

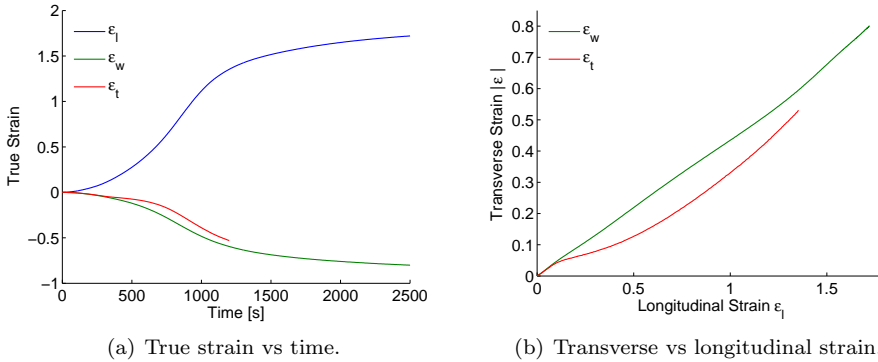


Figure 4.5: (a) True strain in the length, width and thickness directions versus time and (b) Transverse strain versus longitudinal strain for T-PP-00-1.

Figure 4.5 (a) gives the true strain in the length, width and thickness directions against time for the test T-PP-00-1. This test is chosen as a representative test to show the behaviour of the material. The reason why the ϵ_t is stopped at an earlier time than the other strains is because voids started to form on the side of the test specimen making it impossible for the DIC software to correlate the pictures. The deformed polypropylene from the side after the voids started to form can be seen in Figure 4.6. The strains in the width and thickness directions starts off equal, however after about 500 s they start to deviate, with smaller strains in the thickness direction. The transverse versus longitudinal strain curves in Figure 4.5 (b) also starts with the same gradient. Then, however, the strains in the width continues quite linearly while the thickness strains starts to deviate before increasing almost linearly again. It can be seen that the material experiences a slight volume change.

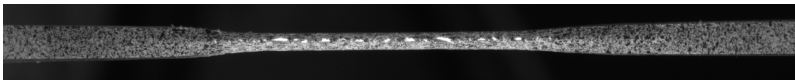


Figure 4.6: Deformed polypropylene from the side.

4.2.2 PP10

In Figure 4.7, it can be seen that the true stress-strain curves of the 10 % fibre reinforced PP differs greatly from the unreinforced PP. Figure 4.7 (a), (b) and (c) shows the three repetitions in the 0, 45 and 90 degree directions respectively and (d) shows the chosen representative tests plotted against each other.

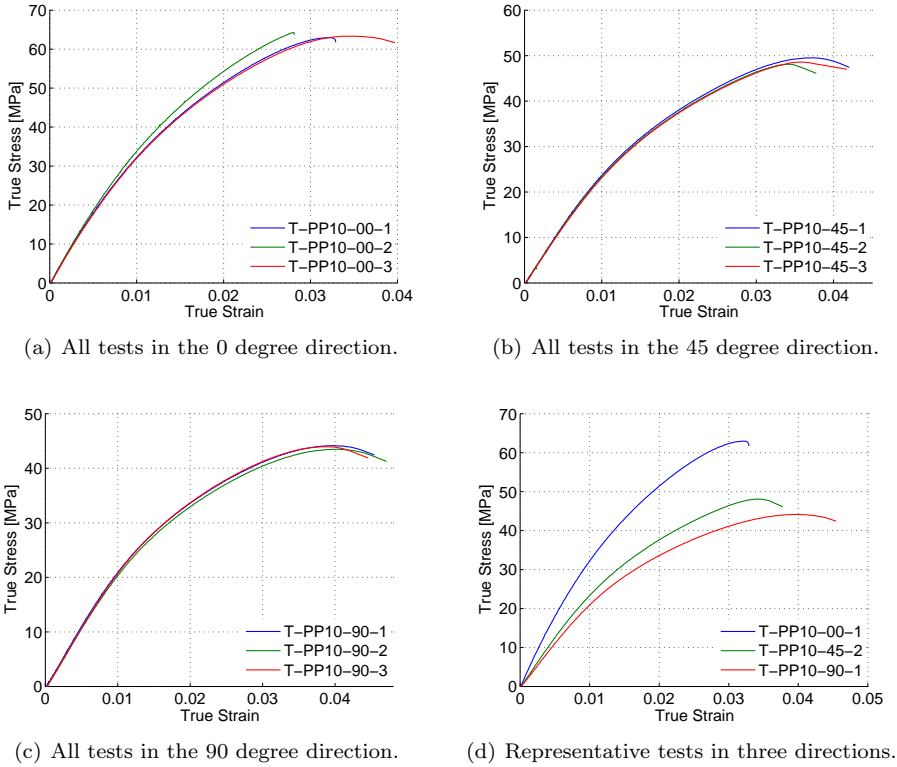


Figure 4.7: True stress-true strain curves for the PP10 tension tests.

From Figure 4.7(d) it can be seen that the material exhibits anisotropic behaviour. The tensile tests performed in the 0 degree direction has a higher strength than the ones done in the 45 and 90 degree direction. This suggests that most of the fibres are aligned with the 0 degree direction and the material will therefore have a higher strength in this direction. The results shows that adding 10 % fibres changes the material response greatly. The resulting glass fibre reinforced material displays brittle behaviour, while the unreinforced PP displays ductile behaviour. The material has a tensile strength of approximately 63 MPa in the 0 degree direction and 49 MPa and 44 MPa in the 45 and 90 degree directions respectively. The tensile strength was measured at the maximum force. The tensile strain was 3.4 %, 4.1 % and 4.6 % in the 0, 45 and 90 degree directions respectively. These were averages

of the three tests and the results for each test can be found in Table B.2 for the tensile strength and B.3 for the tensile strain. The Young's modulus was measured to be 3501 MPa in the 0 degree direction, which is more than double the modulus found for PP. In the 45 and 90 degree directions, the average Young's modulus was 2494 MPa and 2183 MPa respectively. The Young's modulus for each test is found in Table B.1.

Figure 4.8 (a) shows the true strain in the length, width and thickness directions plotted against time for the representative test T-PP10-00-1. The true strains in the with and thickness directions are not completely equal as have been assumed when using Equation (4.9). The difference between the three true stress curves were, however, so small that this could be neglected. Figure 4.8 (b) shows the magnitude of the transverse strain versus longitudinal strain for T-PP0-00-1. The curve shows a liner relationship between ε_l and ε_w , and an almost linear relationship between ε_l and ε_t . This shows that there are no significant volume change during testing. The values for the true strains will differ in the 45 and 90 degree directions, however, the shape of the curves are the same.

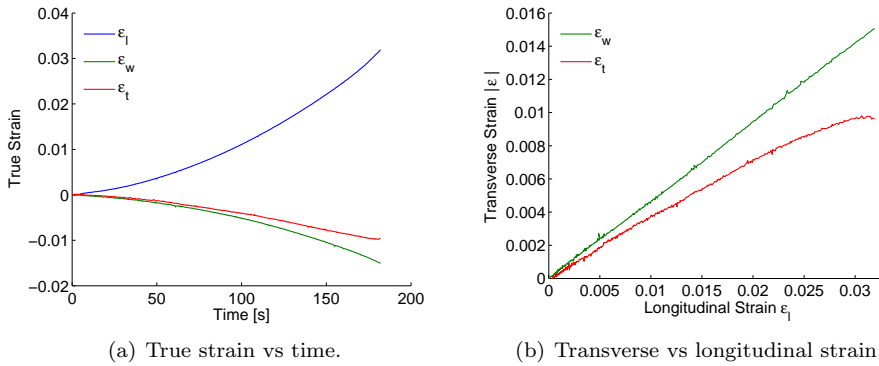


Figure 4.8: (a) True strain in the length, width and thickness directions versus time and (b) Transverse strain versus longitudinal strain for T-PP10-00-1.

4.2.3 PP30

The results from the tension tests with a 30 % fibre concentration can be seen in Figure 4.9. Firstly the three repetitions in the 0, 45 and 90 degree directions have been presented in Figure 4.9 (a), (b) and (c) respectively, and in Figure 4.9(d), the three representative tests in each material direction has been presented.

From Figure 4.9 (d) it can be seen that adding more fibres gives a stronger and more brittle material. Also these tests show an anisotropic behaviour in the material. The results show that adding more fibres makes the material more brittle, and the PP10 material is much closer to the PP30 material than the unreinforced PP.

The average tensile strength was found to be 90 MPa in the 0 degree direction, 55 MPa in the 45 degree direction and 48 MPa in the 90 degree direction. This gives almost a doubling in the tensile strength from the 90 to the 0 degree direction. The average tensile elongation at break was 2.5% in the 0 degree direction. In the 45 and 90 degree directions it was 3.8% and 3.2% respectively. Contrary to the PP10 material, here the material in the 45 degree direction has the highest tensile strain. The average Young's modulus is 6415 MPa, 3188 MPa, and 3015 MPa in the 0, 45 and 90 degree directions respectively. The tensile strength, strain and Young's modulus for each repetitions can be found in Table B.2, B.3 and B.1 respectively.

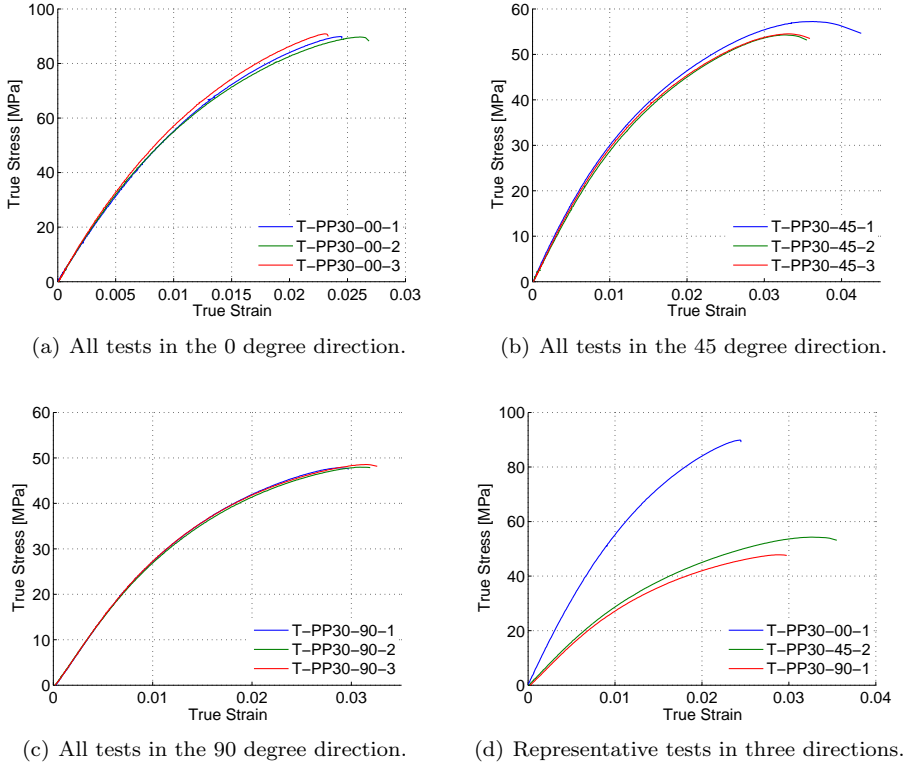


Figure 4.9: True stress-true strain curves for the PP30 tension tests.

Figure 4.10 (a) shows the strain in the length direction ε_l , width direction ε_w , and thickness direction ε_t versus time for the representative test T-PP30-00-1. This shows that ε_w and ε_t are not equal as have been assumed when using Equation 4.9, they are however close enough so that it did not make a significant difference in the true stress-strain curve. The transverse strain versus longitudinal strain in Figure 4.10 (b) shows a nearly linear curve. This shows that there are no significant volume change during testing.

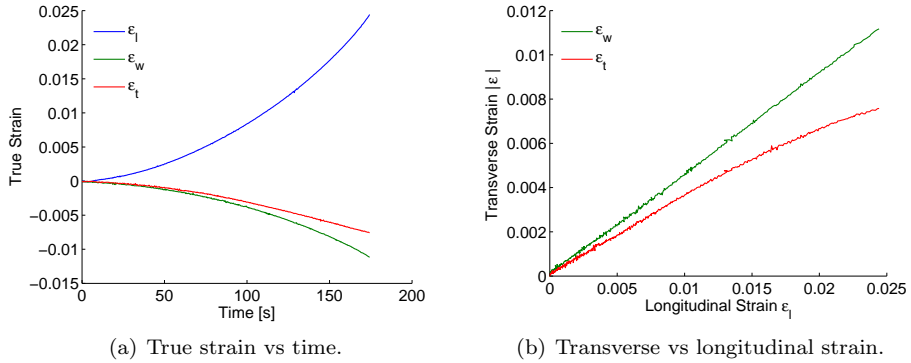


Figure 4.10: (a) True strain in the length, width and thickness directions versus time and (b) Transverse strain versus longitudinal strain for T-PP30-00-1.

4.2.4 Comparison and discussion

Figure 4.11 shows a comparison of the true stress-strain curves obtained from the three materials in the 0 degree direction. The curves of the glass fibre reinforced materials show high strength levels and low deformation capabilities. PP10 and PP30 presents brittle behaviour with a failure strain of about 3.5% and 2.5% respectively, whereas unreinforced PP presents ductile behaviour. The figure also shows clearly that the increase in fibre content leads to an increase in tensile strength and elastic modulus.

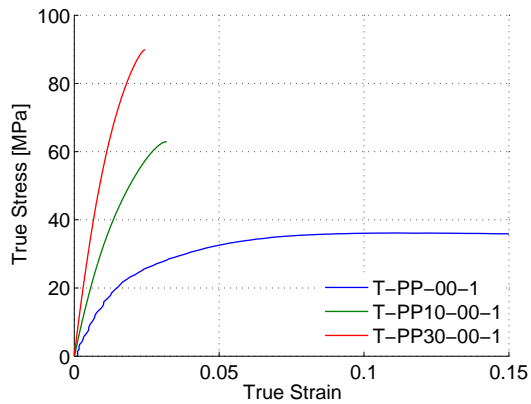


Figure 4.11: True stress-strain curves showing the three materials in the 0 degree direction.

The same can be seen in Figure 4.12 which shows the representative tests of the three materials in the 45 and 90 degree directions.

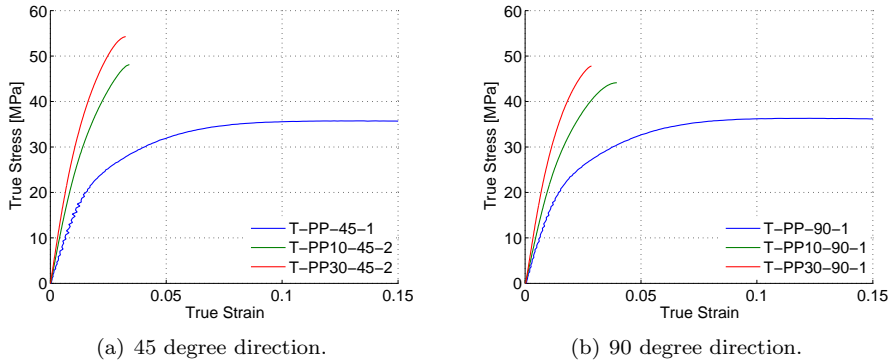


Figure 4.12: True stress-strain curves showing the three materials in the 45 and 90 degree direction.

The difference in tensile strength is most noticeable in the 0 degree direction, this suggests that the fibres are mostly aligned in the longitudinal direction. The materials also get a higher stiffness and strength in the 45 and 90 degree directions, however, the increase in fibre content is not as effective as in the 0 degree direction.

Figure 4.13 shows the average elastic modulus found from the linear region of the three repetitions of each test versus the fibre concentration in the materials. The Elastic modulus found for each test can be found in Table B.1 in the appendix.

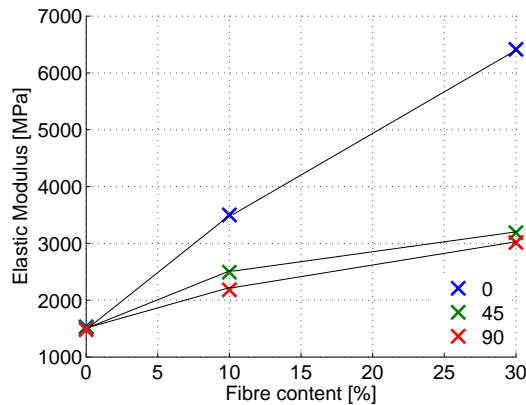


Figure 4.13: Elastic modulus vs fibre content.

Especially in the 0, and 90 degree directions it can be seen that there is almost a linear relationship between the elastic modulus and the fibre content. Only tests on three different materials is not enough to conclude with this linear relationship. Some studies have shown that the elastic modulus of glass fibre reinforced polypropylene increase linearly up to about 40% fibre concentration and then an

increase in fibre has less effect [2].

Figure 4.14 clearly shows the ductile behaviour of PP and the brittle fracture observed in the PP10 and PP30 tests. There is no necking before fracture in either PP10 or PP30. The glass fibres can be seen in the fracture area in Figure 4.14 (b) and (c). It is difficult to tell from the specimens in which directions the fibres are aligned. The fracture is not completely straight.

Figure 4.15 (b) and (c) shows that the fibre reinforced specimens in the 45 degree direction presents an oblique fracture. The PP specimen in Figure 4.15 (a) presents the same behaviour as in the 0 degree direction. Looking closely at 4.15 (b), it can be seen that the 10 % fibre reinforced material has some quite long fibres.

The fracture in the 90 degree direction for PP10 and PP30, shown in Figure 4.16 (b) and (c), is straight across the specimen as in the 0 degree direction, however, a much cleaner fracture is observed. PP in Figure 4.16 (a) still exhibits the same behaviour as in the 45 and 0 degree direction.

These three different fracture patterns in the three directions suggests that the fracture mechanisms in the three directions are different.

The results found in this section shows that the fibre reinforced polypropylene and the unreinforced polypropylene are two different classes of materials. PP is ductile and isotropic while PP10 is brittle and anisotropic.

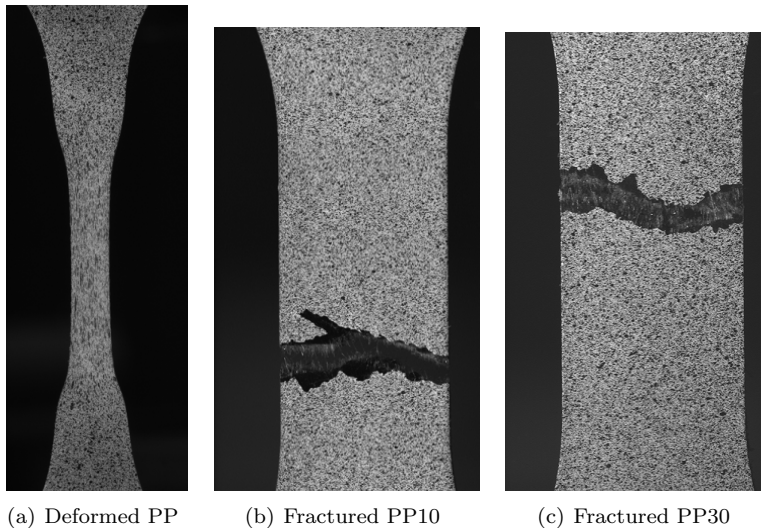


Figure 4.14: Figures showing the deformed tensile specimens of (a) PP, (b) PP10 and (c) PP30 in the 0 degree direction.

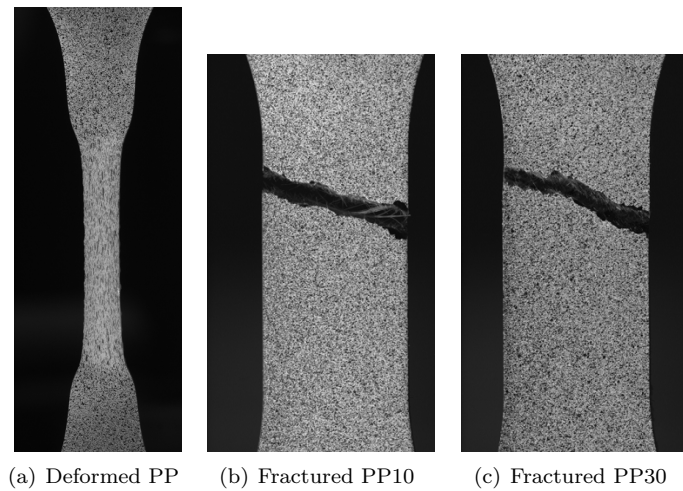


Figure 4.15: Figures showing the deformed tensile specimens of (a) PP, (b) PP10 and (c) PP30 in the 45 degree direction.

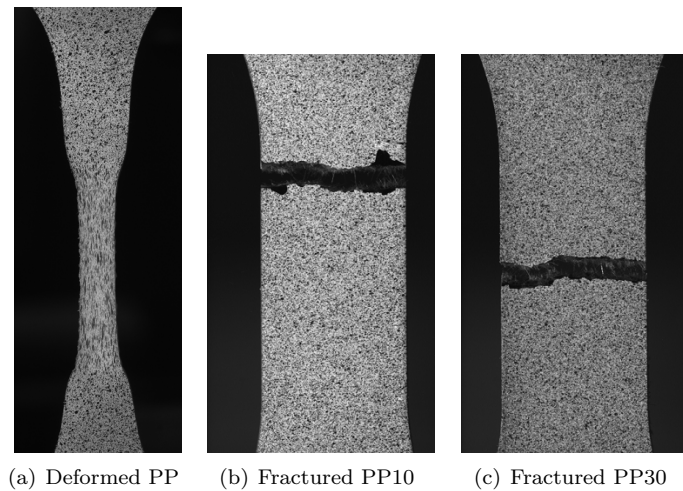


Figure 4.16: Figures showing the deformed tensile specimens of (a) PP, (b) PP10 and (c) PP30 in the 90 degree direction.

4.3 Bending tests

The bending tests were performed in two material directions, 0° and 90° with respect to the moulding direction.

For brittle materials that have approximately linear behaviour in tension, the fracture stress may be estimated from the failure load in a three-point bending test by simple linear elastic beam analysis shown in Equation (4.10).

$$\sigma = \frac{Mt}{2I} \quad (4.10)$$

Here, M is the bending moment, t is the thickness of the bending specimen and I is the area moment of inertia about the neutral axis. For a rectangular cross section of width w and thickness t , $I = wt^3/12$. In this case, the highest bending moment occurs at midspan and is $M = PL/4$, where P is the load and L is the span length. Equation (4.11) gives the stress at fracture.

$$\sigma_{fb} = \frac{3L}{2wt^2}P_f \quad (4.11)$$

P_f is the fracture force in the bending test. σ_{bf} is usually identified as the bend strength or the flexural strength [1].

Brittle materials are usually stronger in compression than in tension.

The elastic modulus may also be obtained from the bending test. For a three-point bending problem, linear-elastic analysis gives the maximum deflection as:

$$v = \frac{PL^3}{48EI} \quad (4.12)$$

The value of the flexural or bending modulus E may then be calculated from the slope dP/dv of the initial linear portion of the load versus deflection curve [1].

$$E = \frac{L^3}{48I} \left(\frac{dP}{dv} \right) = \frac{L^3}{4wt^3} \left(\frac{dP}{dv} \right) \quad (4.13)$$

Ideally the flexural modulus of elasticity should be equivalent to the tensile modulus of elasticity. In reality, these values are often different, especially for plastic materials.

The results of the bending tests will be presented as force-displacement curves. The force is taken directly from the cross-head of the machine. The displacement is also taken from the cross head of the machine and adjusted for any offset between the wedge and test specimen. A representative test, here test B-PP30-00-1, was tested to see whether it would be most correct to use the displacement from the cross head or node displacement from DIC, and it was found that the results were almost equal.

4.3.1 PP

The bending tests, as well as the tensile tests, shows no significant variation depending on test direction, as can be seen in Figure 4.17. The material reaches a

maximum force of slightly under 250 N with small variations in the repetitions. These small variations can be due to the small differences in test specimen geometry, shown in Table A.2. The curves are initially linear before the gradient decreases slightly and the maximum force is reached. Then the force decreases slightly until fracture.

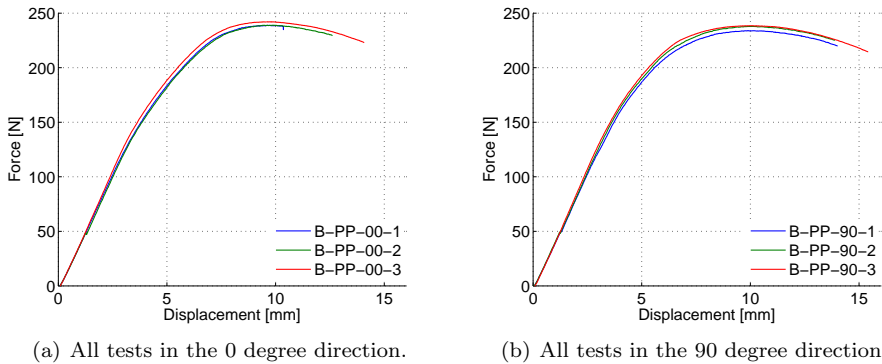


Figure 4.17: Force-displacement curves of the bending test for PP.

The average flexural modulus found from Equation (4.13) were 2230 MPa in the 0 degree direction and 2175 MPa in the 90 degree direction. The difference between the directions is not larger than the difference within the three repetitions, and therefore the material is most likely isotropic in bending as well. This Young's modulus is larger than the one found from the tensile tests. The flexural modulus for each test can be found in Table B.4 The flexural strength found using Equation (4.11) was $\sigma_{fb} = 77$ MPa in the 0 degree direction and $\sigma_{fb} = 73$ MPa in the 90 degree direction. Here also the difference in flexural strength is small enough to still assume that material direction is not the reason for the deviation. The Young's modulus and flexural strength found from the bending tests for each repetition is found in Table B.5.

4.3.2 PP10

Figure 4.18 shows the results of the bending tests of the PP30 material. These tests shows clearly the anisotropic nature of the material with a higher maximum force in the 0 degree direction. The material breaks almost immediately after the maximum force has been reached. The displacement at fracture is much lower for PP10 than for PP. The flexural Young's modulus found to be approximately 4400 MPa and the flexural strength was 110 MPa in the 0 degree direction, and the flexural modulus and strength was 3144 MPa and 86 MPa respectively in the 90 degree direction.

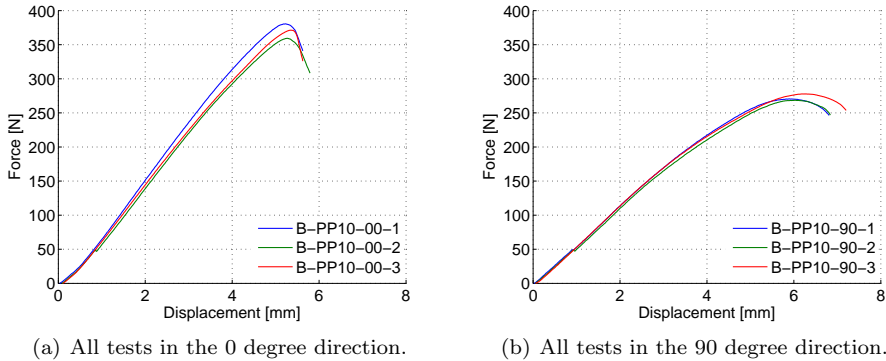


Figure 4.18: Force-displacement curves of the bending test for PP10.

4.3.3 PP30

Figure 4.19 shows the force-displacement curves of the PP30 material. The maximum bending force in the 90 degree direction is half of that in the 0 degree direction. This suggests that increasing the fibre concentration increases the anisotropic nature of the material. This material also breaks right after the peak stress has been reached, at a displacement much lower than that of PP, but close to that of PP10.

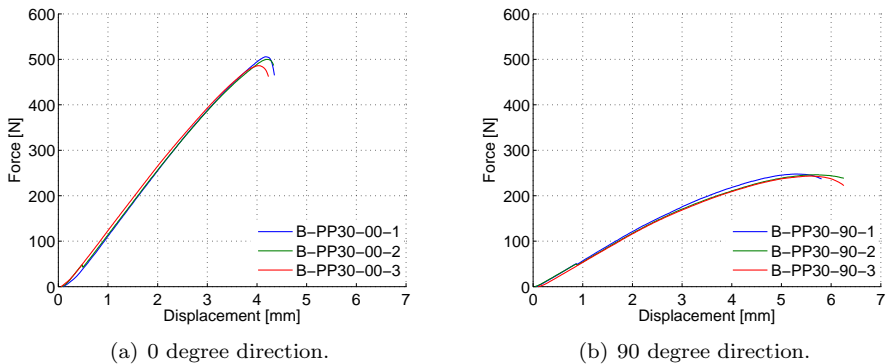


Figure 4.19: Force-displacement curves of the bending test for PP30.

4.3.4 Comparison and discussion

For all materials, some of the repetitions had a small kink in the beginning of the force-displacement curve. This is in the raw data from the machine, and looking at the pictures in DIC, it can be explained by the test specimen moving slightly horizontally before continuing to move downwards.

The bending test in the 0 degree direction shows as expected a substantial increase in the force with increasing fibre content, as can be seen in Figure 4.20 (a). Figure 4.20 (b) shows that the fibre reinforcement in bending is not very effective in the 90 degree direction. The maximum force does not increase much, for PP30 barely anything, and the ductility is reduced. The slope of the curves of PP10 and PP30 in the 90 degree direction is almost equal, and PP10 is the material that reaches the highest force.

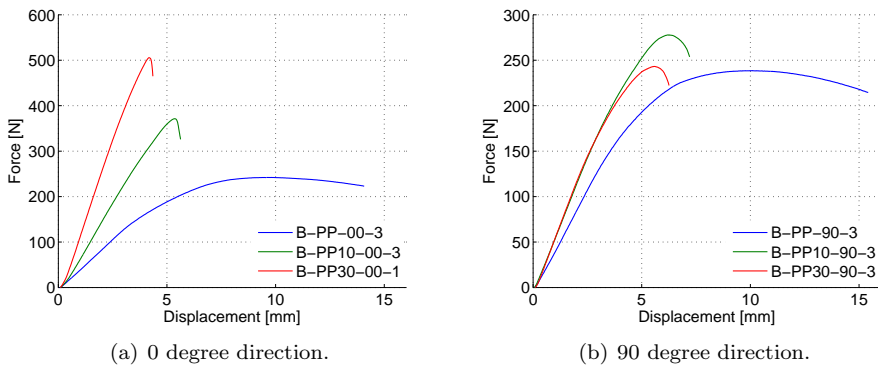
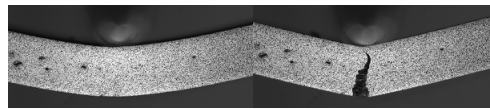
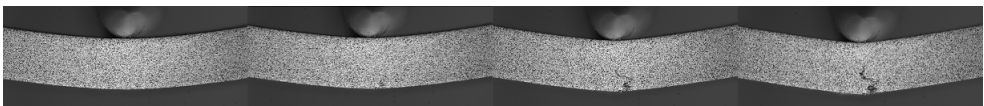


Figure 4.20: Force-displacement curves of the representative bending tests.

Figure 4.21 shows the difference in the fracturing between the PP10 and PP30 materials in the 0 degree direction. While for PP10, the specimen fractured over almost the whole thickness at once, for PP30 the fracture through the thickness was more gradual. More glass fibre in PP30 held the specimen together longer as not all the fibres break simultaneously.



(a) PP10 in the 0 degree direction.

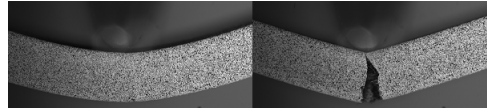


(b) PP30 in the 0 degree direction.

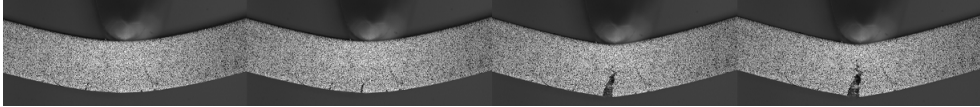
Figure 4.21: Figures showing (a) PP10 fracturing and (b) PP30 fracturing.

As seen in Figure 4.22, the tests in the 90 degree direction also have a different fracture pattern in PP10 and PP30. The PP10 material breaks all through the

thickness at the same time, and the PP30 material experiences a more gradual crack growth. The crack grows slightly faster in the 90 degree direction for PP30 than in the 0 degree direction.



(a) PP10 in the 90 degree direction.



(b) PP30 in the 90 degree direction.

Figure 4.22: Figures showing (a) PP10 fracturing and (b) PP30 fracturing.

Figure 4.23 shows the bending modulus of elasticity versus the fibre content. The average values of the three repetitions were used, and the values for each test can be found in Table B.4. The tests performed in the 0 degree direction shows an almost linear relationship between the elastic modulus and the fibre content, as could also be seen in the tensile results. This is as expected from the literature, a study on the properties of injection moulded long fibre PP at high fibre content found that the flexural modulus increased linearly in the glass fibre content range of 0-73 wt%. The Young's modulus determined in tensile testing deviated from linearity at fibre contents higher than 40 wt% [2]. In the 90 degree direction however, increasing the fibre content from 0 % slightly increases the elastic modulus, further increasing the fibre concentration does not make the material stiffer, the bending modulus actually decreases slightly.

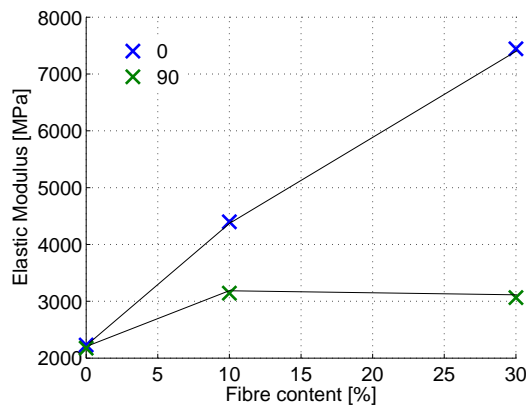


Figure 4.23: Bending elastic modulus vs fibre content.

4.4 Plate with centric hole

Figure 4.24 shows the plate specimen with mesh from the DIC. A vector of initial length $L_0 = 25$ mm has been added to show where the displacement measure has been taken from. This vector spans 5 mm in on each side of the centric hole of diameter 15 mm. This vector was chosen to be able to compare the results with the validation tests in Chapter 6.

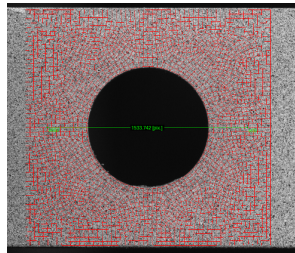


Figure 4.24: DIC mesh on the plate with a centric hole.

4.4.1 PP

The complex nature of the plate with a centric hole compared to a tensile test makes the PP fracture at a much lower displacement than in the tensile tests. As shown in Figure 4.25, the force reaches a maximum force of about 1200 N for the first and second repetition and 1350 N for the third repetition, before it decreases slightly until fracture. This is due to the ductility in the material. The plate with a centric hole has a much shorter gauge length than that of the tensile specimen, and therefore, a shorter length has to take up most of the strains, and make the material fracture earlier. The third repetition acts different from the two first repetitions, this is due to difference in the strain rate.

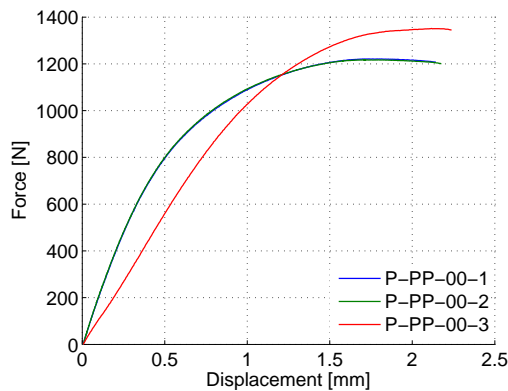


Figure 4.25: Force-displacement curves of plate tests for PP.

The third repetition has a higher strain rate than the two first repetitions. This makes the material act quite different as it gives it a lower stiffness, but a higher maximum force.

4.4.2 PP10

PP10 breaks at a much lower displacement than PP, as can be seen in 4.26. The maximum force is also higher at a value between 1650 and 1700 N for the first and second repetition and just under 2000 N for the third repetition. The displacement at fracture is approximately 0.7 mm for the first and second repetition and 0.65 mm for P-PP10-00-3. In this test, the third repetition has a higher maximum force, and a steeper curve than the two other repetitions because of the difference in strain rate. The third repetition has a higher strain rate than the other repetitions, this gives the material a higher stiffness and strength, and it fractures at a slightly lower displacement.

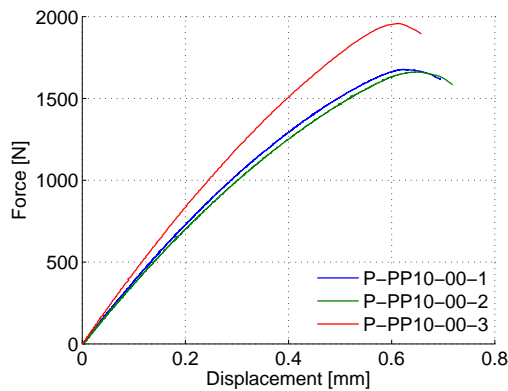


Figure 4.26: Force-displacement curves of plate tests for PP10.

4.4.3 PP30

Figure 4.27 shows the force displacement curves for PP30. It can be seen that the materials shows brittle behaviour with a lower maximum displacement and a higher maximum force than the two previous materials. The maximum force is approximately 2300 N for the first and second repetition and about 2500 N for the third repetition. The displacement at fracture is approximately 0.55 mm for the first and second repetition and 0.5 for the third. Also in this test, the third repetition with a higher strain rate gives a higher maximum force and a higher stiffness. It also fracture at a slightly lower displacement than the first and second repetitions.

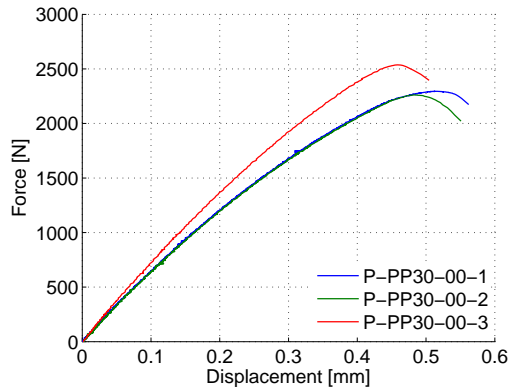


Figure 4.27: Force-displacement curves of plate tests for PP30.

4.4.4 Comparison and discussion

The third repetition for each material is different than the others. This is due to a difference in strain rate. Figure 4.28 shows the force-time relationship for the three repetitions for the PP30 material. This shows that the first and second repetitions and the third repetition differ in test time with about a factor of 10. Whereas the first and second repetitions fracture at a time of approximately 700 s, the third repetition fracture at 70 s. The same force-time relationship could be seen in the PP and PP10 tests.

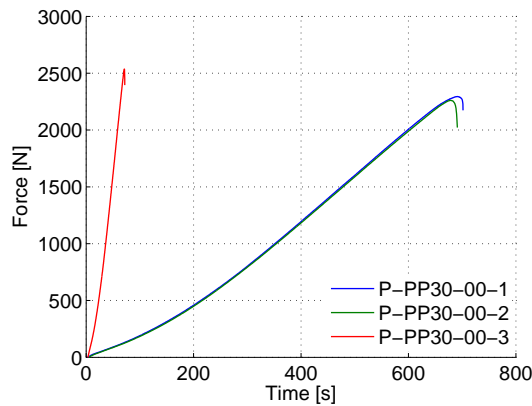


Figure 4.28: Force-time curves of plate tests for PP30.

If we assume most of the 0.5 mm displacement in the force-displacement curve of P-PP30-00-3 occurred in a gauge length of approximately 7.5 mm on each side of the hole with a test time of 70 s, the strain rate can be calculated as:

$$\dot{\epsilon} = \frac{0.5}{7.5} = 9.52 \times 10^{-4} \text{s}^{-1} \approx 10^{-3} \text{s}^{-1} \quad (4.14)$$

Making the same assumptions for the first and second repetitions gives a strain rate of almost a 10th of the third repetition at $\dot{\epsilon} \approx 10^{-4} \text{s}^{-1}$. The same can be found for the tests of the PP and PP10. These results show that the material is in fact strain rate-dependent even though this is not assumed in the material model calibrated and validated in Chapters 5 and 6 respectively.

Figure 4.29 shows the three representative tests chosen for each material. The third repetition was chosen as the representative test for each material as this was the test performed at the same strain rate as the uniaxial tensile tests and bending tests.

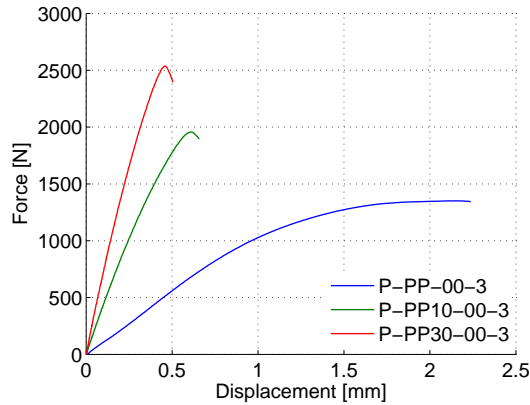


Figure 4.29: Force-displacement curves of the representative plate tests.

The brittle versus ductile behaviour in the fibre reinforced PP versus the unreinforced PP can be seen clearly from the curves. The curves show the same relationship between the three materials as have been seen in the uniaxial tensile tests and bending tests in the 0 degree direction.

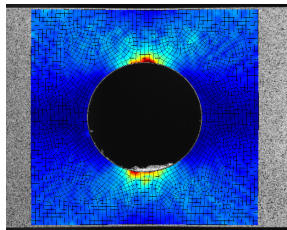


Figure 4.30: Strain field on the plate specimen of PP30.

Figure 4.30 shows the strain field from DIC on the place specimen in the PP30

material. This strain pattern was similar in the PP and PP10 materials as well. The figure shows that the strain is largest nearest the edges of the hole on each side of the hole. This was where the fracture initiated in all the tests and then it spread to the edges.

4.5 Summary

The observations from the experimental tests can be summed up in the following points:

- An increase in the glass fibre content shows an increase in the stiffness and strength of a material. PP is ductile while PP10 and PP30 is brittle. This is most noticeable in the 0 degree direction, but can also be seen in the 45 and 90 degree direction for the uniaxial tensile test. For the bending test in the 90 degree direction, the stiffness and strength increased from PP to PP10, then however it decreased when using PP30.
- When introducing fibre reinforcements, the material becomes anisotropic. The material has the highest stiffness and strength in the 0 degree direction with a lower strength in the 45 and 90 degree directions. Increasing the fibre content increases the stiffness and strength greatly in the 0 degree direction, however, the effects are smaller in the 45 and 90 degree direction.
- The fracture pattern in the tensile tests is different in the three material directions. While it is straight across the specimen in the 0 and 90 degree directions, it is oblique in the 45 degree direction. There also seems to be some differences between the 0 and 90 degree direction with a cleaner fracture in the 90 degree direction. In the bending tests, there largest difference was between the two fibre reinforced materials. Whereas in the PP10 material the crack grows instantly over the whole thickness, the crack growth in the PP30 material was more gradual. For PP30 the crack grew slightly faster in the 90 degree direction than in the 0 degree direction.
- The plate tests were performed at two different strain rates. This showed that the all materials were strain rate dependent.

Chapter 5

Calibration

This chapter explains and exemplifies the calibration of the material model. The SIMLab ductile polymer model has been tested on several different polymers, including polypropylene, a number of times. The brittle polymer model for fibre reinforced polymers, however, is quite new and needs more testing. This chapter will deal with calibration of a material model for the 30% fibre-reinforced polypropylene. This material was chosen since this is the grade mostly used for industry purposes. This material is anisotropic and therefore the results in each material direction is needed. The calibration process will begin by identifying 15 non-zero coefficients that describe parts of the material behaviour. These parameters have been explained further in Section 2.4 and an overview of the required parameters can be found in Table 5.1. These parameters will then be implemented in a numerical model to be compared with the experimental results in Chapter 4. Some parameters can not be found directly from the material tests and these will be calibrated in a parametric study. In this section, the representative tests chosen in Chapter 4 is used to calibrate the model. These are T-PP30-00-1, T-PP30-45-2 and T-PP30-90-1.

5.1 Parameters

A set of base parameters had to be selected in order to calibrate the material model. These parameters were found using the results from the tensile tests performed. Nine anisotropic material parameters had to be found to satisfy the orthotropic SIMLab brittle polymer model. These were three Young's moduli, three Poisson's ratios and three shear moduli. Then the damage parameters could be selected with a normal distribution of the fracture parameter κ_0 . Approximate numbers for κ_{0min} and κ_{0max} can be found from the tensile test results in the reference direction. κ_0 , κ_{0std} , and G_f however have to be found by trial and error. Values will be chosen in this section and refined in the parametric study. A total of 15 values have to be selected to make the material card for the SIMLab polymer model and an overview of these can be found in Table 5.1.

Table 5.1: Overview of coefficients required in the material model.

Material parameters	
Young's modulus	E_X
	E_Y
	E_Z
Poisson's ratio	ν_{XY}
	ν_{YZ}
	ν_{ZX}
Shear modulus	G_{YZ}
	G_{ZX}
	G_{XY}
Damage parameters	
Exponent	a
Fracture energy	G_f
Brittle damage threshold	κ_0
Minimum value of κ_0	κ_{0min}
Maximum value of κ_0	κ_{0max}
Standard deviation of κ_0	κ_{0std}

Since no tests were performed in the out-of-plane direction, it is not possible to know how the material will perform in this direction. If we assume that through the injection moulding the fibres have been aligned in the 0 degree direction, further on called the X-direction, both the Y-axis (90 degrees) and Z-axis will be perpendicular to the fibres. Because of this it can be further assumed that the material is transversely isotropic. This will make $E_Y = E_Z$, $\nu_{YZ} = \nu_{ZX}$ and $G_{ZX} = G_{XY}$ as well as make G_{YZ} dependent on E_Y and ν_{YZ} :

$$G_{YZ} = \frac{E_Y}{2(1 + \nu_{YZ})} \quad (5.1)$$

This is further explained in Section 2.4.1.

5.1.1 Material parameters

Young's modulus

Young's modulus can be found by taking a linear fit to the elastic region of the true stress-strain curves from the tensile tests. This was done for the tests in the 0° and 90° directions. Since the Young's modulus is difficult to get accurately from tensile tests, it was decided to use an average from all three tensile tests in each direction. The resulting Young's moduli were found to be $E_X = 6415$ MPa and $E_Y = 3015$ MPa. The value in the 0° direction is slightly lower than the suppliers value of $E = 6650$ MPa. Since no tensile tests have been performed in the Z-direction and

transverse isotropy has been assumed, the Young's modulus in the Z-direction is set equal to that of the Y-direction, namely $E_Z = 3015$ MPa.

Poisson's ratio

Poisson's ratio was determined from the transverse and longitudinal strain in the elastic area, as seen in Equation (5.2).

$$\nu = -\frac{\varepsilon_w}{\varepsilon_l} \quad (5.2)$$

Figure 5.1 shows the transverse strain versus the longitudinal strain in the reference tests in the 0 and 90 degree directions. Poisson's ratio is set to be the slope of the curves for $\varepsilon_l < \sim 0.01$. The values $\nu_{XY} = 0.45$ is found from T-PP30-00-1 and $\nu_{YZ} = 0.19$ is found from T-PP30-90-1. The assumption of transverse isotropy gives $\nu_{ZX} = 0.19$.

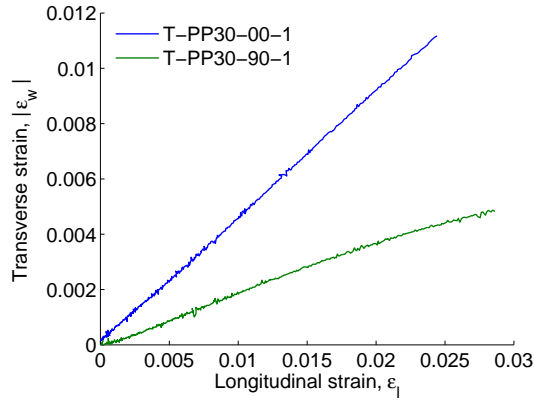


Figure 5.1: Transverse versus longitudinal strain for the reference tests in the 0 and 90 degree directions.

Shear modulus

No shear tests were performed, therefore it is not possible to get the shear modulus directly from the tests without making some assumptions. It has been assumed that the material is transverse isotropic and this entails that the shear modulus in the Y-Z-plane is dependent on the Young's modulus in the Y-direction and the Poisson's ratio in the Y-Z-plane. This relationship can be seen in Equation (5.1). Using this yields $G_{YZ} = 1267$ MPa. G_{XY} and G_{ZX} are still unknown, but equal. They have been set to an arbitrary value of 1000 MPa as they do not affect the tensile results and it is not possible to know if it is correct.

5.1.2 Damage parameters

Exponent a

The exponent a is the exponent found in Equation 2.7. For tensile tests it is found that a suitable value is 2, and since the calibration is done with the help of the uniaxial tensile tests and the validation process is done on a tensile test on a plate with a centric hole. This parameter will not be a part of the subsequent parametric study.

Minimum and maximum value of κ_0

The minimum value of κ_0 can be approximated by looking at the reference tensile test performed in the 0 degree direction along the fibres. This value can be set where the curves gradient starts to decrease slightly from the initial elastic straight line. It is difficult to see exactly where this is as the curve is almost continuously curved. κ_{0min} was found by plotting the true stress-strain curve along with the Young's modulus found above and see where they deviated. κ_{0max} can be physically represented by the true stress strain curve as the point of fracture. In Figure 5.2, the locations of κ_{0min} and κ_{0max} is plotted with the reference curve.

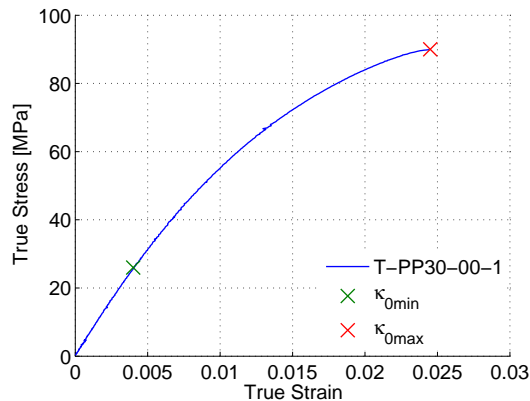


Figure 5.2: True stress-strain curve of T-PP30-00-1 showing from where κ_{0min} and κ_{0max} were chosen.

The values were found to be $\kappa_{0min} = 0.004$ and $\kappa_{0max} = 0.0245$.

Brittle damage threshold κ_0

The brittle damage threshold κ_0 is more difficult to find directly from any curves. This has to be found through trial and error. A preliminary value of κ_0 was chosen to be the middle value between κ_{0min} and κ_{0max} . The chosen value was then $\kappa_0 = 0.01425$.

Standard deviation of κ_0

The standard deviation κ_{0std} is also difficult to find from the true stress-strain curves. It was decided to set one standard deviation between the minimum value and the threshold κ_0 . The resulting value is then $\kappa_{0std} = 0.01025$.

Fracture energy G_f

From Figure 2.6 in Section 2.4.2 it can be seen that the fracture energy is the area underneath the graph divided by the fracture area for a cubical area. The fracture energy G_f is defined as

$$G_f A_e = \frac{1}{2} E_0 \kappa_0 \kappa_1 V_e \quad (5.3)$$

where $A_e = h_e^2$ is the fracture area for the cubical element and $V_e = h_e^3$ is the volume. h_e is the characteristic length of the cubical finite element. This energy is invariant to the element size and is assumed to be a material property. Increasing G_f will increase the parameter κ_1 . The Fracture energy is supposed to be a material property, however investigations into this has showed that this is not the case. The fracture energy is set to an arbitrary value of 10 N/mm.

5.1.3 Parameters base model

The final values chosen to be tested in a numerical model is shown in Table 5.2.

Table 5.2: Overview of the coefficients chosen for first trial

Material parameters	
E_X	6415 MPa
E_Y	3015 MPa
E_Z	3015 MPa
ν_{XY}	0.45
ν_{YZ}	0.19
ν_{ZX}	0.19
G_{YZ}	1270 MPa
G_{ZX}	1000 MPa
G_{XY}	1000 MPa
Damage parameters	
a	2
G_f	10 N/mm
κ_0	0.01425
κ_{0min}	0.004
κ_{0max}	0.0245
κ_{0std}	0.01025

5.2 Numerical model

In this section the material model is applied in the finite element software Abaqus. Only the uniaxial tensile tests will be treated in this chapter. This section will give a short review of the modelling process and the results for the preliminary parameters found in the previous section.

The tensile specimen were modelled using the nominal geometry found in Figure 3.2. The thickness was set to be 2.76 mm. Only a quarter of the model was modelled with symmetry about the Y-axis and Z-axis to decrease the calculation time. The shoulders of the test specimen have been shortened to only take into account the part between the clamps.

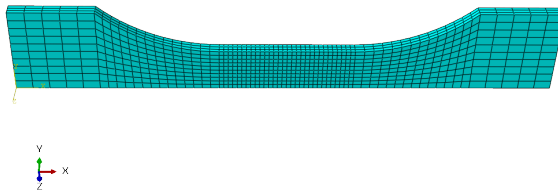


Figure 5.3: Abaqus model of tensile specimen with mesh.

The applied geometry is shown in Figure 5.3. Fully integrated solid, 8-node linear brick elements were used, called C3D8 in Abaqus. Full integration was used as tests using reduced integration exhibited hourglass modes. An element size of approximately $0.5 \text{ mm} \times 0.5 \text{ mm} \times 0.5 \text{ mm}$ was used in the parallel area with larger elements on the shoulders. This gave approximately 30 elements in the in the length of the gauge area, 10 in the width and 3 elements in the thickness for the quarter model. This mesh size seemed to be the most optimal with regards to accuracy and computational expense.

The left and right ends were defined as node sets representing the clamps in the test machine. All degrees of freedom were fixed at the left end, and the translations in the Y and X-direction as well as all rotational degrees of freedom were fixed at the right end. A constant velocity in mm/s was applied in the X-direction at the right end.

The specimen was modelled as an explicit model in Abaqus/Explicit. This is mostly used for dynamic problems, and the tensile tests were performed under quasi-static conditions. To be able to model this test as explicit, time-scaling had to be used in order to limit the computational effort. Time-scaling could be used as opposed to mass-scaling since the materials model applied is not strain rate sensitive. The analysis time was set to 0.1 s. This value seemed to give a low kinetic energy and

thereby small dynamic effects. The velocity on the right side of the specimen was set to 13 mm/s and maintained constant throughout the analysis. A smooth step amplitude was also introduced to the velocity to achieve a nearly static response at steady state, similar to that in Abaqus/Standard [13].

A material orientation had to be introduced to be able to represent the anisotropic behaviour of the material. A local coordinate system was introduced and connected to the material orientation to easily be able to change the material direction from the 0 degree direction to the 45 and 90 degree directions. The local coordinate system has, as the global coordinate system, the X-axis in the longitudinal direction and the Y-axis in the transverse direction. The Z-axis is in the thickness direction.

5.2.1 Base model

The resulting base models are shown in engineering stress versus engineering strain curves. The gauge area of the numerical model is modelled with nominal lengths while the experimental specimens differ slightly. The engineering strains were found for the experimental test by superimposing a vector of length $L_0 = 15$ mm in the middle of the parallel area in the DIC and extracting the engineering strain directly. In the Abaqus model, the displacement between two nodes 15 mm apart were measured to get the elongation of the gauge area. This elongation was converted into engineering strain by $\varepsilon_{eng} = \Delta L/L_0$. The engineering stress was calculated from the force and the initial gauge area as seen in Equation 4.3, for both the experimental and numerical tests. The resulting engineering stress-strain curves for the 0 degree direction can be seen in Figure 5.4.

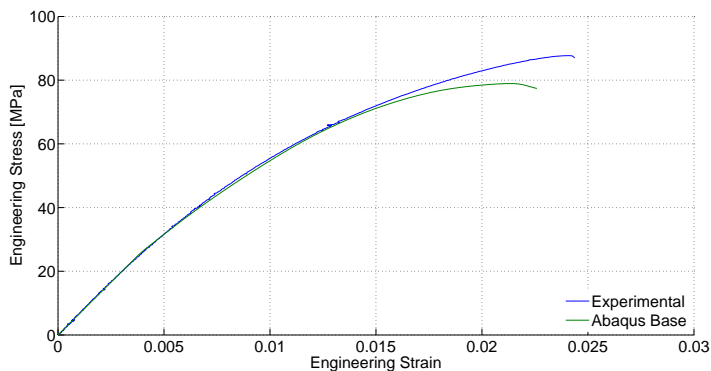


Figure 5.4: Engineering stress-strain showing the experimental results versus the base model in the 0 degree direction.

The base model follows quite well up to about $\varepsilon_{eng} = 0.015$. The initial elastic modulus seems to be correct. The model is slightly lower than the experimental after about $\varepsilon_{eng} = 0.006$ and it is not able to predict the maximum stress.

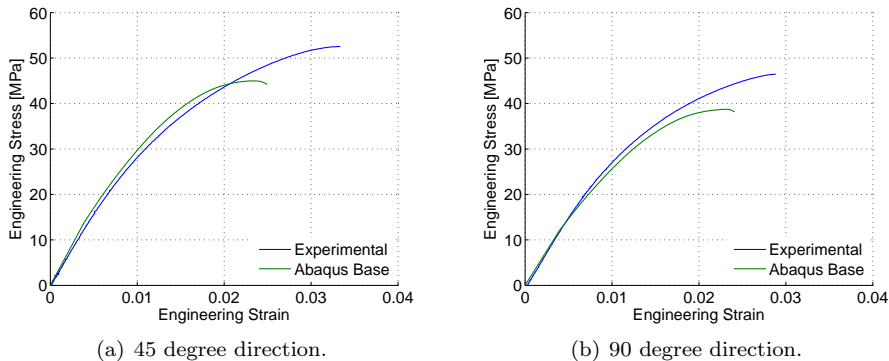


Figure 5.5: Engineering stress-strain curves showing the abaqus model and experimental results in the 45 and 90 degree direction.

Figure 5.5 show the results in the 45 and 90 degree direction. None of the models can predict the maximum stress. The stiffness in the 45 degree test is too high. The numerical model in the 90 degree direction has a slightly lower stiffness than the experimental. Otherwise the curves follows experimental curves to some extent.

The curves show that the base model, although not perfect, does predict the anisotropy of the material quite well. The parametric study in the next section will try to improve the parameters in order to get the models to predict the maximum stresses.

5.3 Improvement of Material Parameters

5.3.1 Parametric study

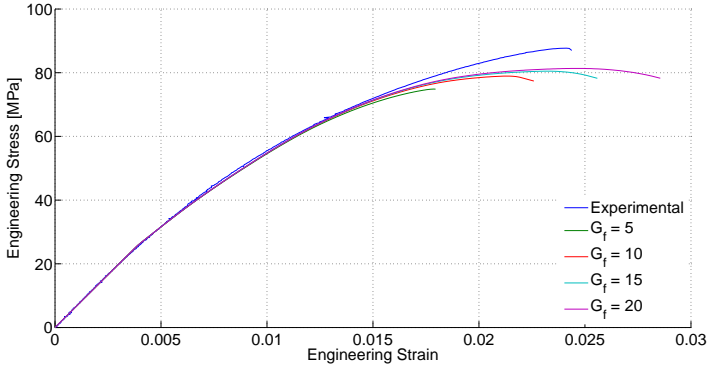
From the previous section it can be seen that the base material model was not close enough to the experimental results. The stiffness in the 0 degree direction seemed to be satisfactory. Three of the parameters were chosen almost at random, therefore these are the ones that should be changed first to see how they affect the results. To isolate the effect of each parameter, only one parameter will be changed at a time. Table 5.3 shows an overview of the parametric study with the values used in the base model in bold. The parametric study was done on the material in the 0 degree direction as this is the direction principally reinforced by the fibres. The exception is the E_Y and G_{YZ} which were changed in the 90 and 45 degree directions respectively.

Table 5.3: Parametric Study.

Fracture Energy G_f	5	10	15	20
Brittle damage threshold κ_0	0.01	0.01425	0.015	0.02
Standard deviation κ_{0std}	0.008	0.01025	0.015	0.02
Minimum κ_{0min}	0.002	0.004	0.005	
Maximum κ_{0max}	0.0245	0.03	0.035	0.05

Fracture energy

Figure 5.6 shows how changing the fracture energy affects the engineering stress-strain curves of the numerical model. Increasing the Fracture energy increases the strain where the maximum force occurs. It seems that the chosen value of 10 is too low, and this could therefore be increased to get a better material model.

**Figure 5.6:** Engineering stress-strain curve varying G_f .

Brittle damage threshold κ_0

Figure 5.7 shows that increasing κ_0 will make more elements fail at a higher strain level, which lifts the curve. The base model, with $\kappa_0 = 0.01425$ is a good starting point. $\kappa_0 = 0.01$ makes the curve much too low, and $\kappa_0 = 0.02$ too high. A value of $\kappa_0 = 0.015$ is the best match to the experimental curve up to about $\varepsilon_{eng} = 0.011$, however, after that the slope decreases too early. To be able to model the maximum stress, increasing κ_0 can be an alternative, however, the other measures have to be taken to lower other parts of the curve.

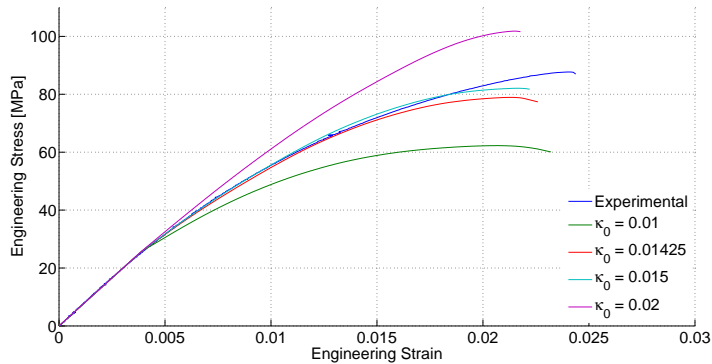


Figure 5.7: Engineering stress-strain curve varying κ_0 .

Standard deviation of κ_0

A higher standard deviation will make more elements fail earlier while decreasing it elevates the curve by making more elements fail later. Almost doubling the standard deviation from $\kappa_{0std} = 0.01025$ to $\kappa_{0std} = 0.02$ does not have a large effect. Changing other parameters along with the standard deviation can make the effect larger. In the base model, κ_{0min} and κ_{0max} is set at one standard deviation from κ_0 . Changing the standard deviation will raise and lower the normal distribution curve shown in Figure 2.8. Increasing κ_{0std} will lower the normal distribution, and while still 68.28 % of the elements will fail within one standard deviation, the cut of values κ_{0min} and κ_{0max} will be less than one standard deviation from κ_0 . The opposite is true if the standard deviation decreases.

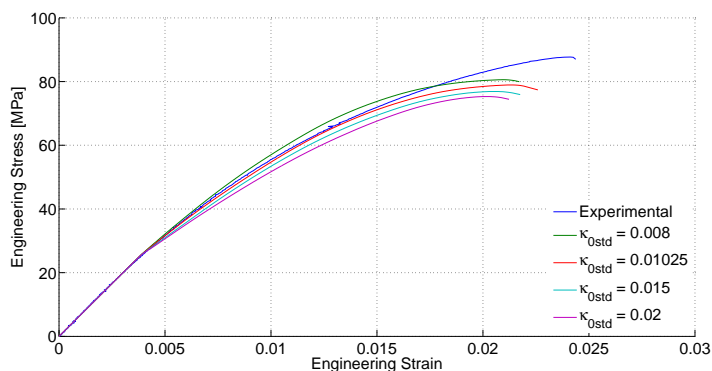


Figure 5.8: Engineering stress-strain curve varying κ_{0std} .

Minimum value of κ_0

Changing κ_{0min} will change where the first elements will start to fail and the curve stops being linear, as can be seen in Figure 5.9. With the chosen stiffness, it seems that the base model represents the curve the best. With $\kappa_{0min} = 0.002$ the elements starts to fail too early, and with $\kappa_{0min} = 0.005$ too late.

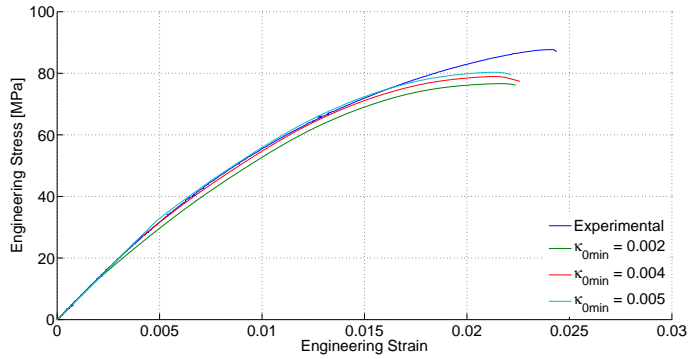


Figure 5.9: Engineering stress-strain curve varying κ_{0min} .

Maximum value of κ_0

Figure 5.10 shows that increasing κ_{0max} raises the latter part of the curve slightly. Because of the dependence on the κ_{0std} and κ_0 , a κ_{0max} above 0.03 with the current κ_{0std} and κ_0 is unnecessary as it will not make any significant change to the curve. The base value of κ_{0max} is set to be at one standard deviation. Increasing the cut off value κ_{0max} will be effective up to a certain point, however, above this point, most of the elements will already have failed when reaching κ_{0max} . Either changing κ_{0std} or κ_0 while changing κ_{0max} will give a larger effect on the response.

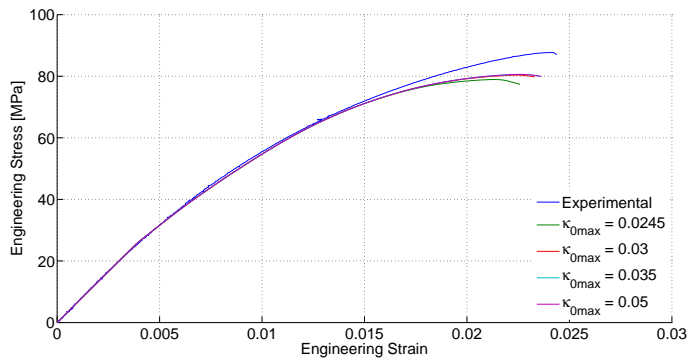


Figure 5.10: Engineering stress-strain curve varying κ_{0max} .

Young's modulus, E_Y and shear modulus, G_{YZ}

The stiffness in the 90 degree direction in the numerical model was lower than that in the experiment. Therefore it was decided to increase this to $E_Y = 3100$ MPa which seemed to fit better. Since the Shear modulus in the Y-Z-plane in a transversely isotropic material is dependent on E_Y , this was also changed according to Equation (5.1). Checking the numerical model in the 45 degree direction showed that this gave a much higher stiffness than in the experiments. Therefore, after a few test runs, it was found that a $G_{YZ} = 1100$ MPa gave a result that closer matched the experiment. Figure 5.11 (a) shows the curve in the 90 degree direction with the base and new value of E_Y , and (b) shows the engineering stress-strain curves in the 45 degree direction with different values for G_{YZ} .

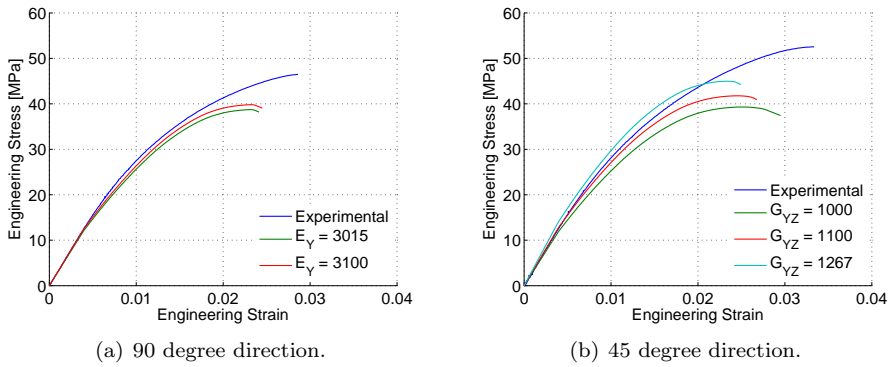


Figure 5.11: Engineering stress-strain curves showing (a) variation in E_Y in the 90 degree direction and (b) variation in G_{YZ} in the 45 degree direction.

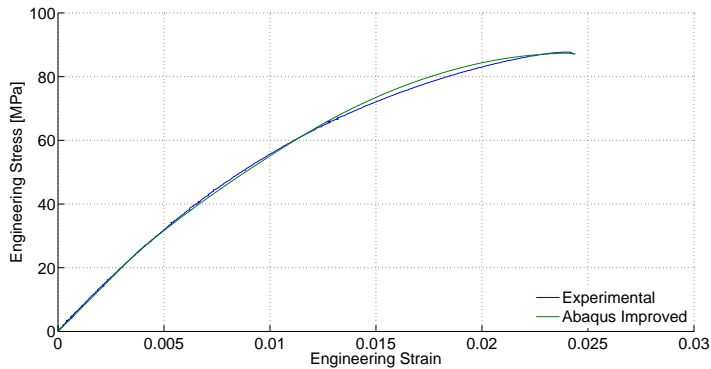
5.3.2 Improved Model

After seeing how the parameters altered the numerical response, a few tests were run and eventually an improved model was found. The parameters used in the improved model can be seen in Table 5.4. The stiffness in the X-direction has been kept from the base model as well as the Poisson's ratios. The base model revealed that the stiffness in the 45 and 90 degree directions were not satisfactory, therefore these have been changed through G_{YZ} and E_Y . The fracture energy has been increased to make the model fracture later. The brittle damage threshold has also increased to get a higher maximum stress, and the standard deviation of κ_0 has been increased to compensate for the increase in κ_0 . The maximum value of κ_0 has also increased to make the curve fail later. κ_{0min} has been kept from the base model as this value seemed to be the best fit.

Table 5.4: Overview of the coefficients chosen for improved model.

Material parameters	
E_X	6415 MPa
E_Y	3100 MPa
E_Z	3100 MPa
ν_{XY}	0.45
ν_{YZ}	0.19
ν_{ZX}	0.19
G_{YZ}	1100 MPa
G_{ZX}	1000 MPa
G_{XY}	1000 MPa
Damage parameters	
a	2
G_f	11 N/mm
κ_0	0.016
κ_{0min}	0.004
κ_{0max}	0.03
κ_{0std}	0.0125

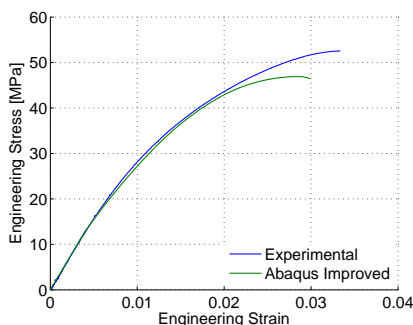
The improved curve in the 0 degree direction is presented in Figure 5.12 along with the experimental curve of T-PP30-00-1. It was difficult to make a curve that represents the experimental curve exactly. However, after several trials an improved curve was made. This curve overestimates the stress slightly between a strain of 0.012 to 0.023. It follows the rest of the curve quite well and the initial stiffness seems to be a match.

**Figure 5.12:** Engineering stress-strain showing the experimental results versus the improved model in the 0 degree direction.

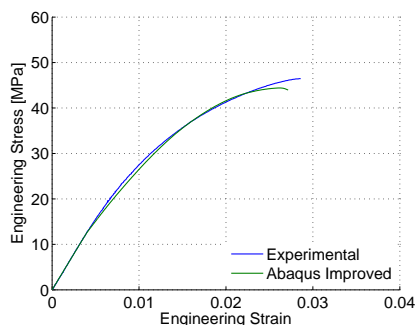
In the 45 degree direction, shown in Figure 5.13 (a), the improved curve under-

estimates the stress throughout except for the initial stiffness. It severely underestimates the maximum stress and maximum strain. Disregarding the maximum stress and strain, the improved model seems to follow the experimental stress quite well up to 0.02 engineering strain. This shows that the model represents the orthotropic nature of the material quite well. The improved model is better than the base model.

Figure 5.13 (b) shows that in the 90 degree direction, the improved curve is a major improvement to the base curve. However, it underestimates the stress in certain areas and it never reaches the maximum stress and strain from the experiments. The material model is a good fit up to an engineering strain of about 0.025. The new stiffness seems better and disregarding the models inability to predict the maximum stress and strain in the 45 and 90 degree directions, it does represent the orthotropic material well. The model in the 90 degree direction reaches a maximum stress and strain which is closer to the experimental than the model in the 45 degree direction.



(a) 45 degree direction.



(b) 90 degree direction.

Figure 5.13: Engineering stress-strain curves showing the improved FE-model and experimental results in the 45 and 90 degree direction.

5.4 Comparison and discussion

In general, the improved material model manages to represent 30 wt% glass fibre reinforced polypropylene well. There are, however, some deviations. In this section the results are compared and discussed.

There are only two major components in the brittle material model, and that is elastic anisotropy and brittle damage. It was possible to fit the material parameters quite well in all directions since these parameters were dependent on the material direction. The material model was able to represent the initial stiffness of all the tests. In the 0 degree direction, the material model followed the experimental curve well. The model was able to represent strains up to approximately

0.02 and 0.025 in the 45 and 90 degree directions respectively. The model deviates quite much in the end of the curve in the 45 degree direction, and the FE-model in the 90 degree direction also struggled to predict the maximum stress and strain.

The latter parts of the curves are more dependent on the damage parameters than the material parameters. The material parameters were dependent of the material direction, however, the damage parameters were taken from the reference test in the 0 degree direction. Figure 5.14 shows the fracture in one of the tests of PP30 in the three material directions. This shows that the fracture in the 45 degree direction is oblique while the fracture in the 0 and 90 degree directions is approximately perpendicular to the longitudinal direction. There is also a much cleaner fracture in the 90 degree direction than the 0 degree direction. This suggests that there are different fracture mechanisms involved in the fractures in the different directions. Therefore, the damage parameters should also be dependent on the material direction to correctly predict the fracture in the 45 and 90 degree directions.

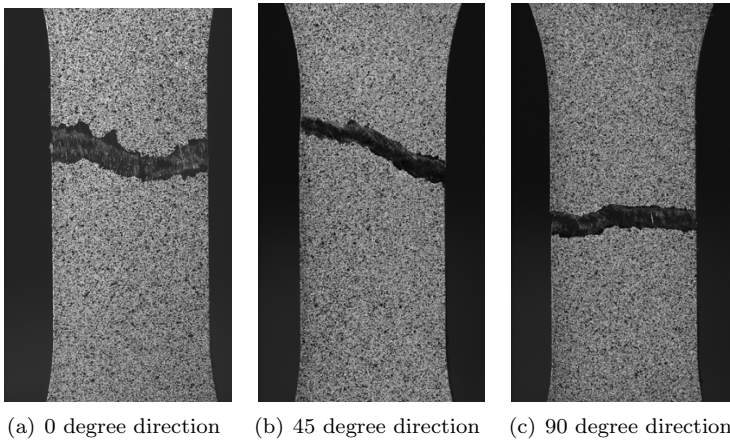


Figure 5.14: Figures showing the deformed tensile specimens of PP30 in each directions.

There are several uncertainties in the material model applied as not enough tests were performed to conclusively determine all the material parameters. Transverse isotropy was assumed as the material tests did not provide all the parameters in the material card, and this seemed like a reasonable assumption for a fibre reinforced polymer. This assumption might not be correct, and since the new shear modulus in the Y-Z-plane G_{YZ} was not dependent on E_Y , this is something that should be investigated. For this purpose, the uniaxial tensile tests should be performed in the out-of-plane direction as well. Shear tests should also be conducted to remove the uncertainty in the shear moduli. Compression tests could also be performed to detect if there is any difference in the compressive strength and tensile strength. The bending tests gave a higher flexural Young's modulus than the tensile Young's

modulus. This could suggest that there is a difference in compression and tension, and therefore this should be investigated further.

Several of the parameters changed in the parametric study shifted the curves similarly. Both increasing the fracture energy and κ_{0max} made the model fracture later. Increasing the κ_0 and decreasing κ_{0std} both lifted the curve. The resulting shape of the curve when changing the different parameters were slightly different, and finding a resulting curve with the exact shape of the experimental was difficult since all the statistical damage parameters were dependent on each other.

Chapter 6

Validation

In this chapter, the material model created in the previous chapter will be validated. The validation test applied is a tension test using a plate with a centric hole. The main objective of a validation test is to test a wide range of the properties of the calibrated material model. The experimental test setup and results can be found in Chapter 3 and 4 respectively. This chapter will focus on the implementation of the material model on numerical models of the test in Abaqus.

6.1 Plate with centric hole

This test was chosen because of its pure and simple loading. In spite of the simple loading the load response is more complex and gives good information about how the material model manages to represent more complex deformations than those found in the calibration test.

6.1.1 Numerical model

The plate with a centric hole was modelled in much the same manner as the uniaxial tensile test in Chapter 5. The plate was modelled as a quarter of the nominal geometry given in Figure 3.6 with symmetry about the Y and Z-axis to reduce computational time. The specimen was modelled using only the gauge length, which was given by approximately 14 mm on each end of the hole. The total thickness of the specimen, before symmetry, was set to be 2.76 mm, the same as the tensile specimen. Figure 6.1 shows the Abaqus model of the quarter plate specimen with the chosen mesh.

Fully integrated solid elements called C3D8 in Abaqus were used. These were the same elements used for the tensile specimen in the previous chapter. An element size of approximately 1 mm × 1 mm × 1 mm was used on the entire model. A smaller size of 0.5 mm × 0.5 mm × 0.5 mm was tested, this however increased the computational time substantially and did not give a different force-displacement response.

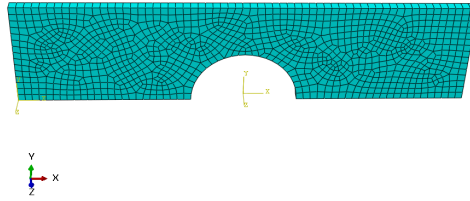


Figure 6.1: Abaqus model of a quarter of the plate specimen with mesh.

The specimen was fixed at the left end, and all degrees of freedom except translation in the X-direction were fixed at the right end. A constant velocity was applied in the X-direction at the right end.

The plate was modelled using Abaqus/Explicit. Time-scaling had to be used to limit the computational effort and a total analysis time of 0.1 s was chosen. This gave a sufficiently low kinetic energy. A velocity of 8 mm/s was applied on the right side with a smooth step amplitude to achieve a nearly static response at steady state.

Since the experimental tests on the plate was only performed in one direction, the validation test can not say anything definite about the anisotropy of the model. The numerical model was, however, modelled with the material orientation connected to a local coordinate system to be able to do the numerical simulation in the 45 and 90 degree directions as well.

The displacement was extracted from nodes 5 mm on each end of the hole making the initial length between them 25 mm.

6.1.2 Base Model

Firstly the numerical model of the plate with a centric hole was modelled with the base parameters found in Table 5.2. This was to see if the base model in the previous chapter was a good starting point for the model, and to be able to see if the improved model calibrated from the parametric study actually showed an improvement in this test as well.

Figure 6.2 shows the Abaqus base model curve plotted with the experimental curve of P-PP30-00-3. The curves are plotted as force-displacement curves. The experimental curve was taken from the experimental results of the plate specimen P-PP30-00-3 in Section 4.4. The displacement was extracted from the difference between two nodes 5 mm from each side of the centric hole initially 25 mm apart. It can be seen that the stiffness of the model seems to be correct and the curve follows very well up to a displacement for about 0.35 mm. The base model is not

able to predict the maximum force and maximum displacement. This was also the case for the base model applied to the tensile tests.

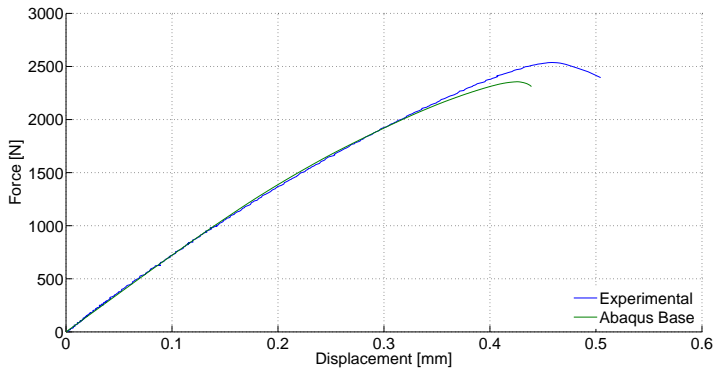


Figure 6.2: Force-displacement curve showing P-PP30-00-3 and the Abaqus base model.

6.1.3 Improved model

Figure 6.3 shows the experimental results of the plate test plotted together with the improved model found from the parametric study in Section 5.3. The parameters used are found in Table 5.4. This curve fits very well with the experimental results. The force is slightly underestimated in the latter part of the curve, however this might be because of slight differences in the nominal dimensions used in the numerical model, and the real dimensions of the experimental test specimen. Altogether the improved model seems to fit the experimental results quite satisfactory.

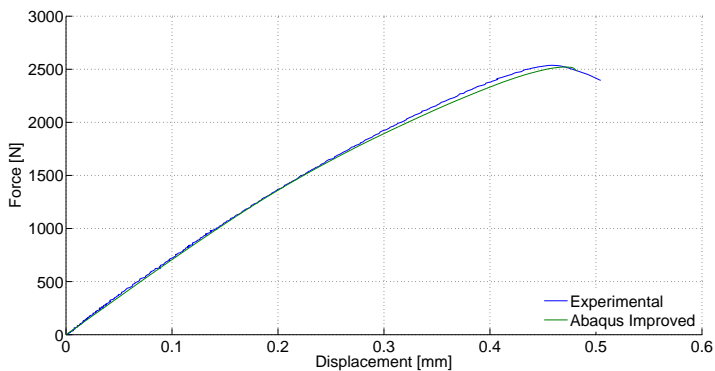


Figure 6.3: Force-displacement curve showing P-PP30-00-3 and the Abaqus improved model.

The validation test has only been performed in one material direction. It is there-

fore not possible to evaluate how the numerical model will perform in relation to the experimental tests in the 45 and 90 degree directions.

6.2 Comparison and discussion

The results of the experimental tests on the plate with a centric hole shows that the material is strain rate dependent, which the material model does not take into account. Therefore, a material model of brittle materials must either be calibrated at the same strain-rate as it will be exposed to in use, or strain-rate needs to be extended to include strain rate.

Figure 6.4 shows the force-displacement curves of the plate with a centric hole found from the numerical model in Abaqus in the 0, 45 and 90 degree direction.

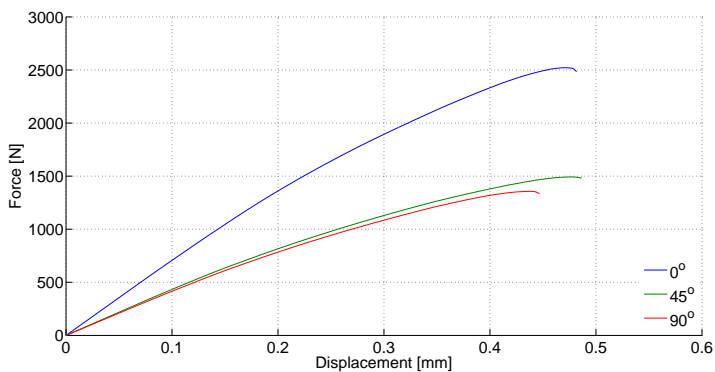


Figure 6.4: Force-displacement curve showing the numerical results in the 0, 45 and 90 degree directions.

The maximum displacement in the 0 and 45 degree directions is approximately equal and in the 90 degree direction it is lower for the numerical models. From the uniaxial tensile tests performed in all material directions, shown in Figure 4.9 (d), it can be seen that the maximum strain in the 45 degrees direction was larger than that of the 90 degree direction, which in turn was larger than in the 0 degree direction. This could suggest that the material model is not able to predict the maximum displacement here either. Otherwise it looks as if the material model may well be representing the 45 and 90 degree direction well, as the stiffness in the 45 degree direction is slightly higher than that in the 90 degree direction and the maximum force is slightly higher in the 45 degree direction. The 0 degree direction reaches a much higher force than the 45 and 90 degree direction, and this can also be seen for the uniaxial tensile tests. This is not possible to know for sure without performing plate tests in these directions.

Figure 6.5 shows the strain field on the experimental test of P-PP30-00-3 in DIC

and the strain field on the numerical model in Abaqus. The general strain field is the same in DIC and Abaqus. The maximum strain is on both sides of the hole with the lowest strain along the centre of the specimens. The numerical model shows some necking, and this can also be seen in the experimental test, although a little less.

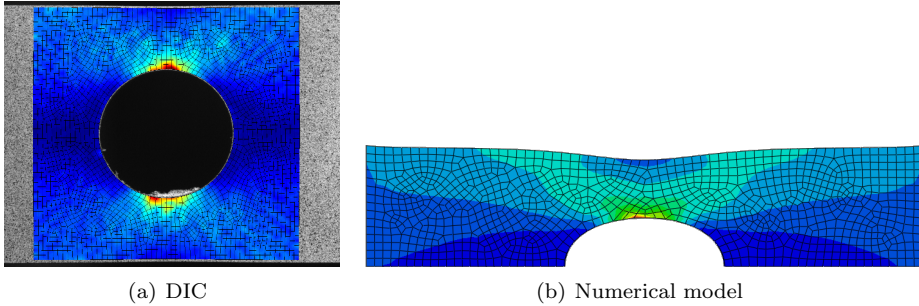


Figure 6.5: The strain field shown on (a) the test specimen in DIC and (b) the numerical model in Abaqus.

6.3 Evaluation of the SIMLab brittle polymers model

Figure 6.6 (a) shows the experimental and numerical results from the uniaxial tensile tests, and (b) shows the experimental and numerical results from the plate tests. The improved material model was used for the numerical results.

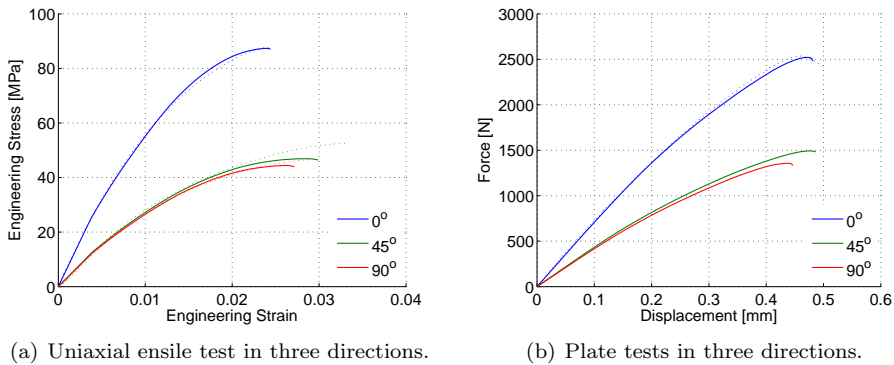


Figure 6.6: Figure showing (a) Engineering stress-strain curves from the experimental and numerical uniaxial tensile tests, and (b) Force-displacement curves from the experimental and numerical plate with a centric hole tests. The experimental results are shown as dotted lines and the numerical results are shown as solid lines.

The results for the calibration and validation tests shows that the current material

model works well in the 0 degree direction. The calibration tests shows that the material still needs some work in the 45 and 90 degree directions. Here it is not able to predict maximum stress and strain. The initial part of the tests are represented quite well. The validation test was only performed in the 0 degree direction, and can therefore not verify the anisotropy results from the calibration test. The numerical results show a similar relationship between the three directions as in the uniaxial tensile tests, and since they fracture at a displacement lower than that of the 0 degree direction, it is likely that also this test is not able to predict the maximum force and displacement.

An improved version of the SIMLab brittle polymers model should also include material direction dependency in the damage parameters as well as the material parameters. The experimental results of the plate with a centric hole in Figure 4.27 shows that the 30 wt% fibre reinforced material is dependent on strain rate. Therefore an improved model should also include strain rate, or it should be specified that the model has to be calibrated with the same strain rate as the part should be subjected to in service.

Chapter 7

Conclusion

In this thesis, polypropylene and glass fibre reinforced polypropylene with a fibre content of 10 % and 30 % by weight have been studied. The mechanical behaviour has been compared for the three materials. Then the SIMLab brittle polymers model was calibrated and validated for the 30 % glass fibre reinforced polypropylene.

Uniaxial tensile tests were performed in three material directions, bending tests were performed in two material directions and a tensile test on a plate with a centric hole was performed in one material direction. The experimental tests revealed that the unreinforced and glass fibre reinforced PP are two different classes of materials. Whereas PP is a ductile polymeric material with isotropic behaviour, the fibre reinforced materials are brittle and anisotropic. PP has a much lower strength and stiffness than PP10 and PP30, and increasing the fibre content from 10 % to 30 % increased the stiffness and strength further.

The brittle material model was calibrated using the uniaxial tensile tests. The improved model found from the parametric study followed the experimental results well in the 0 degree direction. The stiffness in the 45 and 90 degree directions was represented well, however, the model was not able to predict the maximum stress and strain in these directions. When looking at the fracture of the fibre reinforced material, it was seen that the fracture pattern is different in the three directions. Therefore, the damage parameters should probably also be dependent on material directions as the material parameters are.

Experimental tests on the plate with a centric hole showed that all the materials are strain rate dependent. This was not included in the material model used in this thesis. Strain-rate dependence should be included in the material model, as the fibre reinforced material acted very differently under different strain rates. If not, the material model should be calibrated with the same strain rate as the part will have in service.

There were several uncertainties in the material model as not enough material tests were performed to calibrate all the parameters from the tests. Because of this, transverse isotropy was introduced to assume the behaviour in the out-of-plane direction. This seemed to work well as a starting point, however, it is not known how well these parameters will work under other loading conditions than tension.

7.1 Further work

The SIMLab brittle polymer model is new and there are still several aspects of it that needs to be investigated. Some further work that can be done is:

- More material tests can be done to calibrate the material model without having to assume transverse isotropy. This would include tensile tests in the out-of-plane direction as well as shear tests. Compression tests could also be performed to test for any difference in behaviour in tension and compression.
- Micro-computed tomography can be performed to map the actual fibre direction in the material. Tests could also be performed on a material with known fibre length and size.
- Evaluate if fracture development is dependent on the material direction, and if this dependency should be incorporated in the material model. Also evaluate the need to add strain rate dependency in the material model.
- The material model should be tested on other fibre reinforced thermoplastics.
- Perform more validation tests to evaluate other properties than the ones evaluated in this thesis. This could also include tensile tests in other material directions than the 0, 45 and 90 degree directions.
- Perform material tests with fibre reinforced materials with a wider range of fibre concentration to see the influence on fibre concentration. Then test the material model on materials with different fibre content.
- Perform tests to check if the material exhibits viscoelastic properties, and perform tests with loading/unloading to investigate if there are any plastic deformation in the material tests. Tests at different temperatures can also be performed to examine if there is any temperature dependency.

Bibliography

- [1] N. E. Dowling. *Mechanical Behavior of Materials: Engineering Methods for Deformation, Fracture, and Fatigue*. Pearson Education Limited, Edinburgh Gate, Essex, England, 2013.
- [2] J.L. Thomason. The influence of fibre length and concentration on the properties of fibre reinforced polypropylene. 6. The properties of injection moulded long fibre PP at high fibre content. *Composites: Part A*, 36(7):995–1003, 2005.
- [3] S. Kalpakjian and S. R. Schmid. *Manufacturing Processes for Engineering Materials*. Pearson Education, Inc., Upper Saddle River, NJ, USA, 2008.
- [4] K. K. Chawla. *Composite Materials: Science and Engineering*. Springer, 2012.
- [5] W. D. Callister. *Materials Science and Engineering: An Introduction*. John Wiley & Sons, Inc., New York, NY, USA, 2007.
- [6] J. Rösler, M. Bäker, and H. Harders. *Mechanica Behaviour of Engineering Materials: Metals, Ceramics, Polymers, and Composites*. Springer, 2007.
- [7] A. Güllü, A. Özdemir, and E. Özdemir. Experimental investigation of the effect of glass fibres on the mechanical properties of polypropylene (PP) and polyamide 6 (PA6) plastics. *Materials and Design*, 27(4):316–323, 2006.
- [8] M. Vincent, T. Giroud, Clarke A., and Eberhardt C. Description and modeling of fiber orientation in injection molding of fiber reinforced thermoplastics. *Polymer*, 46(17):6719–6725, 2005.
- [9] SIMLab. Theory Manual: SIMLab Polymers Model. SIMLab, Department of Structural Engineering, NTNU, 2013.
- [10] SABIC PP 579S Material Data Sheet. http://plastics.sabic.eu/_scripts/gradeview.pl?template=product&market=a8a28d8c-d0f4-43a7-8798-b0ec5181cc22&gcp_id=94f45742-353a-4f4a-bab4-90cd2bad0736&title=. Accessed: 18-05-2014.
- [11] SABIC STAMAX 30YM240 Material Data Sheet. http://plastics.sabic.eu/_scripts/gradeview.pl?template=product&gcp_id=4a48d8ba-20ec-465f-8156-b3dfc3afaec4&market=4f943736-0fe4-45ec-9993-225e74831e36. Accessed: 18-05-2014.

-
- [12] M. Jerabek, Z. Major, and R.W. Lang. Strain determination of polymeric materials using digital image correlation. *Polymer Testing*, 29(3):407–416, 2010.
- [13] ABAQUS. *Abaqus 6.12 Documentation*. Dessault Systemes, Providence, RI, USA, 2012.
- [14] O. S. Hopperstad and T. Børvik. *Lecture Notes; Material Mechanics*. Structural Impact Laboratory, NTNU, Trondheim, 2013.
- [15] B. et al Mouhmid. A study of mechanical behaviour of a glass fibre reinforced polyamide 6,6: Experimental investigation. *Polymer Testing*, 25(4):544–552, 2006.

Appendix A

Geometrical measurements

A.1 Experimental tests

A Micromar 40EW - IP65 micrometer was used to measure all dimensions except the length and width of the bending specimens and the width of the plate specimens. For these measurements a Mahr Marcal 16EW IP67 digital calliper was used. The micrometer was tightened with three clicks. Some of the plates the specimens were cut out of were not completely level. Especially the bending specimens in the 90 degree direction of PP10 and PP30 were noticeably bent before testing.

The test specimens with lines indicating where the length, with and thickness measurements were taken can be seen in Figures A.1, A.2, and A.3.

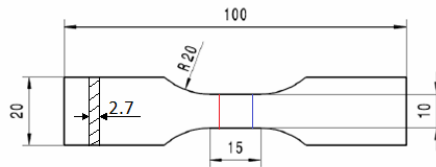


Figure A.1: Nominal geometry of the tensile test specimens with coloured lines showing positions of measurements

The bending specimen were measured two places along the length and three places in the width and thickness, along the coloured lines.

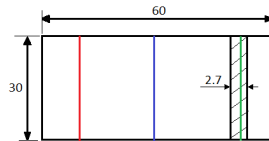


Figure A.2: Nominal geometry of the bending test specimens with indicated markers showing where the measurements were taken.

Because of difficulties measuring the hole, the plate specimens were measured by taking the width on each side of the holes and the width over the whole specimen. The thickness was measured on each side of the hole, at the coloured lines.

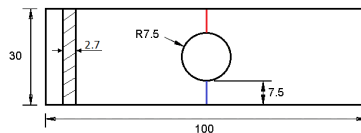


Figure A.3: Nominal geometry of the component test specimens also showing where the measurements were taken.

The measurements are taken from left to right and top to bottom on the test specimens.

Table A.1: Measurements of the tensile specimens before testing [mm].

Specimen name	Width		Thickness	
	1	2	1	2
T-PP-00-1	9.997	9.997	2.788	2.788
T-PP-00-2	9.999	9.998	2.765	2.761
T-PP-00-3	9.996	9.998	2.782	2.783
T-PP-45-1	9.993	9.994	2.761	2.749
T-PP-45-2	9.999	9.995	2.765	2.761
T-PP-45-3	9.999	9.993	2.772	2.763
T-PP-90-1	10.001	10.001	2.776	2.774
T-PP-90-2	10.002	10.001	2.768	2.772
T-PP-90-3	10.000	9.997	2.774	2.764
T-PP10-00-1	9.988	9.989	2.741	2.744
T-PP10-00-2	9.980	9.980	2.721	2.718
T-PP10-00-3	9.968	9.969	2.739	2.740
T-PP10-45-1	9.966	9.970	2.733	2.725
T-PP10-45-2	9.966	9.968	2.727	2.731
T-PP10-45-3	9.973	9.974	2.742	2.734
T-PP10-90-1	9.974	9.976	2.739	2.732
T-PP10-90-2	9.981	9.977	2.744	2.751
T-PP10-90-3	9.976	9.972	2.742	2.748
T-PP30-00-1	9.970	9.969	2.729	2.727
T-PP30-00-2	9.962	9.959	2.764	2.763
T-PP30-00-1	9.983	9.985	2.744	2.744
T-PP30-45-1	9.991	9.988	2.719	2.722
T-PP30-45-2	9.992	9.992	2.724	2.728
T-PP30-45-3	9.997	9.994	2.723	2.721
T-PP30-90-1	9.958	9.957	2.718	2.721
T-PP30-90-2	9.956	9.956	2.724	2.723
T-PP30-90-3	9.960	9.964	2.721	2.721

Table A.2: Measurements of the bending specimens before testing [mm].

Specimen name	Length		Width			Thickness		
	1	2	1	2	3	1	2	3
B-PP-00-1	60.04	60.03	30.06	30.06	30.07	2.753	2.751	2.748
B-PP-00-2	60.00	60.01	30.06	30.06	30.05	2.751	2.763	2.760
B-PP-00-3	60.03	60.01	30.05	30.06	30.05	2.760	2.761	2.760
B-PP-90-1	60.01	59.98	30.06	30.07	30.06	2.763	2.762	2.764
B-PP-90-2	60.02	59.98	30.07	30.06	30.06	2.772	2.768	2.774
B-PP-90-3	59.97	59.99	30.06	30.06	30.06	2.766	2.763	2.770
B-PP10-00-1	60.05	60.02	30.07	30.07	30.08	2.712	2.715	2.718
B-PP10-00-2	60.03	60.00	30.08	30.05	30.03	2.732	2.737	2.738
B-PP10-00-3	59.99	59.99	30.07	30.06	30.06	2.734	2.734	2.734
B-PP10-90-1	60.03	60.04	30.03	30.04	30.05	2.723	2.714	2.713
B-PP10-90-2	60.04	60.04	30.03	30.04	30.04	2.727	2.720	2.720
B-PP10-90-3	60.04	60.04	30.03	30.04	30.03	2.728	2.723	2.737
B-PP30-00-1	59.95	59.96	30.03	30.03	30.04	2.729	2.728	2.730
B-PP30-00-2	59.96	59.96	30.03	30.03	30.06	2.715	2.713	2.714
B-PP30-00-3	59.99	59.97	30.04	30.06	30.05	2.715	2.715	2.715
B-PP30-90-1	60.06	60.07	30.02	30.02	30.03	2.758	2.741	2.737
B-PP30-90-2	60.09	60.09	30.00	30.01	30.02	2.752	2.739	2.738
B-PP30-90-3	60.07	60.07	30.03	30.05	30.03	2.747	2.735	2.735

Table A.3: Measurements of the plate specimens before testing [mm].

Specimen name	Width			Thickness	
	1	2	3	1	2
P-PP-00-1	7.45	7.46	30.05	2.778	2.788
P-PP-00-2	7.45	7.46	30.06	2.770	2.793
P-PP-00-3	7.44	7.44	30.05	2.782	2.783
P-PP10-00-1	7.45	7.44	30.04	2.757	2.746
P-PP10-00-2	7.45	7.44	30.04	2.749	2.760
P-PP10-00-3	7.45	7.44	30.06	2.738	2.732
P-PP30-00-1	7.46	7.45	30.06	2.730	2.730
P-PP30-00-2	7.47	7.44	30.06	2.726	2.731
P-PP30-00-3	7.44	7.45	30.06	2.730	2.740

Appendix B

Experimental Results

This chapter will include some experimental results not included in the main part of the thesis.

B.1 Uniaxial Tensile Tests

The Young's modulus found from the tensile tests were found from the slope of the linear part of the true stress-strain curves found experimentally.

Table B.1: Young's modulus of the materials found from the tensile tests.

Young's modulus, E [MPa]					
Material	Direction	Repetition			Average
		1	2	3	
PP	00	1531	1516	1544	1530
PP	45	1479	1569	1489	1512
PP	90	1451	1449	1541	1481
PP10	00	3421	3665	3417	3501
PP10	45	2555	2499	2427	2494
PP10	90	2204	2158	2188	2183
PP30	00	6230	6390	6626	6415
PP30	45	3270	3136	3158	3188
PP30	90	3079	2979	2987	3015

The stress at yield for PP was taken from the initial stress peak of the true stress-strain curves. The tensile strength for PP10 and PP30 was taken at the maximum stress from the true stress-strain curves.

Table B.2: Stress at yield for PP and tensile strength for PP10 and PP30.

Yield strength / Tensile strength [MPa]					
Material	Direction	Repetition			Average
		1	2	3	
PP	00	36	36	36	36
PP	45	36	36	36	36
PP	90	36	36	36	36
PP10	00	63	64	63	63
PP10	45	50	48	49	49
PP10	90	44	43	44	44
PP30	00	90	90	91	90
PP30	45	57	54	55	55
PP30	90	48	48	49	48

The strain at yield for PP was taken from the initial stress peak in the true stress-strain curve. The tensile strain for PP10 and PP30 was taken at fracture of the true stress-strain curves.

Table B.3: Strain at yield for PP and tensile elongation at break for PP10 and PP30.

Yield strain / Tensile strain [%]					
Material	Direction	Repetition			Average
		1	2	3	
PP	00	10	10	10	10
PP	45	10	10	10	10
PP	90	10	10	10	10
PP10	00	3.3	2.8	4.0	3.5
PP10	45	4.2	3.8	4.2	4.1
PP10	90	4.5	4.7	4.5	4.6
PP30	00	2.5	2.7	2.3	2.5
PP30	45	4.2	3.6	3.6	3.8
PP30	90	3.0	3.2	3.3	3.2

B.2 Bending Tests

The flexural modulus in Table B.4 is found using Equation (B.1), where L is the span length, w is the width of the specimen and t is the thickness of the test specimen. $\frac{dP}{dv}$ is the slope from the linear part of the load-deflection curve for the bending tests.

$$E = \frac{L^3}{4wt^3} \left(\frac{dP}{dv} \right) \quad (\text{B.1})$$

Table B.4: Flexural modulus of the materials found from the bending tests.

Flexural modulus, E [MPa]					
Material	Direction	Repetition			Average
		1	2	3	
PP	00	2213	2180	2295	2230
PP	90	2138	2175	2210	2175
PP10	00	4667	4378	4349	4398
PP10	90	3160	3148	3125	3144
PP30	00	7367	7552	7411	7443
PP30	90	3043	3158	2993	3065

The flexural strength found in Table B.5 is found using Equation (B.2), where L is the span length, w is the width of the specimen and t is the thickness of the test specimen. P_f is the force at fracture in the force-displacement from the bending tests.

$$\sigma_{fb} = \frac{3L}{2wt^2} P_f \quad (\text{B.2})$$

Table B.5: Flexural strength found from bending tests.

Flexural strength, σ_{fb} [MPa]					
Material	Direction	Repetition			Average
		1	2	3	
PP	00	80	77	75	77
PP	90	73	74	71	73
PP10	00	117	104	110	110
PP10	90	84	84	86	85
PP30	00	158	167	159	161
PP30	90	80	80	75	78

Appendix C

Abaqus input files

This appendix contains input files for Abaqus. One representative input file is presented for each of the problems that were modelled. The material cards of the base model and improved model is shown. The material cards from the parametric study in section 5.2 is the same as the base material with one parameter changed at a time. Only one input file from each of the test specimens have been included as the the only difference in the input files of the different tests were the material cards.

C.1 Material cards

A few of the parameters in the materials cards may have a misleading name in regards to their function. This is especially the case for the Poisson's ratios and shear moduli. To clear this up, it has been assumed that:

$$NU_{xx} = \nu_{XY} \quad NU_{yy} = \nu_{YZ} \quad NU_{zz} = \nu_{ZX} \quad (C.1)$$

and

$$G_{xx} = G_{YZ} \quad G_{yy} = G_{ZX} \quad G_{zz} = G_{XY} \quad (C.2)$$

C.1.1 Base Material

```
** MATERIALS
**
*Material, name=SPM
*Density
1.12e-9,
*INCLUDE,INPUT=./DEPVAR_SPM.inc
*USER MATERIAL,CONSTANTS=25
**   EFLAG, YFLAG, RMAPFLAG, FFLAG, HFLAG, VFLAG, TFLAG, DFLAG,
      2,    0,    0,    0,    0,    0,    0,    3
**   STFLAG,  Exx,    NUxx,   Eyy,   NUyy,   Ezz,   NUzz,   Gxx,
      5,  6415,   0.45,  3015,  0.19,  3015,  0.19,  1267
**   Gyy,   Gzz,   dinit,   a,    gf,kappa0, k0min, k0max,
      1000, 1000,    0,    2,    10,0.01425,0.0040,0.0245
**   k0std,
      0.01025,
```

C.1.2 Improved Material

```
** MATERIALS
**
*Material, name=SPM
*Density
1.12e-9,
*INCLUDE,INPUT=./DEPVAR_SPM.inc
*USER MATERIAL,CONSTANTS=25
**   EFLAG, YFLAG, RMAPFLAG, FFLAG, HFLAG, VFLAG, TFLAG, DFLAG,
      2,    0,    0,    0,    0,    0,    0,    3
**   STFLAG,  Exx,    NUxx,   Eyy,   NUyy,   Ezz,   NUzz,   Gxx,
      5,  6415,   0.45,  3100,  0.19,  3100,  0.19,  1100
**   Gyy,   Gzz,   dinit,   a,    gf,kappa0, k0min, k0max,
      1000, 1000,    0,    2,    11,0.0160, 0.0040,0.030
**   k0std,
      0.0125,
```

C.2 Finite element analysis input files

The Abaqus input files have been presented without the geometry part.

C.2.1 Tension test

The input files in the 45 and 90 degree directions are mostly the same as the one for the 0 degree direction except for the orientation part. Therefore, only these lines from the input file for the 45 and 90 tests are shown

0 degree direction

```
*Heading
** Job name: QT-Base Model name: QTension2L-2
** Generated by: Abaqus/CAE 6.12-1
**Preprint, echo=NO, model=NO, history=NO, contact=NO
**
** PARTS
**
*Part, name=Part-1
*Element, type=C3D8
*Nset, nset=Top, generate
*Elset, elset=Top, generate
*Nset, nset=Bot, generate
*Elset, elset=Bot, generate
*Nset, nset=MidSeed
*Elset, elset=MidSeed
*Nset, nset=WholeMod, generate
*Elset, elset=WholeMod, generate
*Nset, nset=Mid
*Nset, nset=Node1
*Nset, nset=Node2
*Orientation, name=Ori-1
           1.,           0.,           0.,           0.,           1.,           0.
3, 0.
** Section: SPM
**Solid Section, elset=WholeMod, orientation=Ori-1, material=SPM
,
*End Part
**
**
** ASSEMBLY
**
*Assembly, name=Assembly
**
**
*Instance, name=Part-1-1, part=Part-1
```

```

*End Instance
**
*Nset, nset=_PickedSet6, internal, instance=Part-1-1, generate
*Elset, elset=_PickedSet6, internal, instance=Part-1-1, generate
*Nset, nset=_PickedSet7, internal, instance=Part-1-1
*Elset, elset=_PickedSet7, internal, instance=Part-1-1
*End Assembly
*Amplitude, name=SmoothStep, definition=SMOOTH STEP
                0.,                0.,                0.01,                1.
**
** MATERIALS
**
**
*include,input=matbase1.inp
**
** BOUNDARY CONDITIONS
**
** Name: BotCon Type: Displacement/Rotation
*Boundary
Part-1-1.Bot, 1, 1
Part-1-1.Bot, 2, 2
Part-1-1.Bot, 3, 3
Part-1-1.Bot, 4, 4
Part-1-1.Bot, 5, 5
Part-1-1.Bot, 6, 6
** Name: ThickSym Type: Symmetry/Antisymmetry/Encastre
*Boundary
_PickedSet7, ZSYMM
** Name: TopCon Type: Displacement/Rotation
*Boundary
Part-1-1.Top, 2, 2
Part-1-1.Top, 3, 3
Part-1-1.Top, 4, 4
Part-1-1.Top, 5, 5
Part-1-1.Top, 6, 6
** Name: WidthSym Type: Symmetry/Antisymmetry/Encastre
*Boundary
_PickedSet6, YSYMM
** -----
**
** STEP: Step-1
**
*Step, name=Step-1, nlgeom=NO
*Dynamic, Explicit
, 0.1
*Bulk Viscosity

```

0.06, 1.2
**
** BOUNDARY CONDITIONS
**
** Name: VelTop Type: Velocity/Angular velocity
*Boundary, amplitude=SmoothStep, type=VELOCITY
Part-1-1.Top, 1, 1, 13.
**
** OUTPUT REQUESTS
**
*Restart, write, number interval=1, time marks=NO
**
** FIELD OUTPUT: F-Output-1
**
*Output, field, number interval=150
*Node Output
RF, U, V
*Element Output, directions=YES
EVF, LE, PE, PEEQ, PEEQVAVG, PEVAVG, S, SDV, STATUS, SVAVG
**
** HISTORY OUTPUT: H-Output-1
**
*Output, history, variable=PRESELECT
**
** HISTORY OUTPUT: RF
**
*Output, history, time interval=0.0001
*Node Output, nset=Part-1-1.Bot
RF1,
**
** HISTORY OUTPUT: Node1
**
*Node Output, nset=Part-1-1.Node1
U1,
**
** HISTORY OUTPUT: Node2
**
*Node Output, nset=Part-1-1.Node2
U1,
*End Step

45 degree direction

*Orientation, name=Ori-1

1., 0., 0., 0., 1., 0.
3, 45.

90 degree direction

*Orientation, name=Ori-1

1., 0., 0., 0., 1., 0.
3, 90.

C.2.2 Plate with centric hole

```
*Heading
** Job name: QP-LM-Base Model name: QPlateHoleLargerMesh
** Generated by: Abaqus/CAE 6.12-1
*Preprint, echo=NO, model=NO, history=NO, contact=NO
**
** PARTS
**
*Part, name=Part-1
*Element, type=C3D8
*Nset, nset=Set-1, generate
*Elset, elset=Set-1, generate
*Nset, nset=Bot
*Elset, elset=Bot
*Nset, nset=Node1
*Nset, nset=Node2
*Nset, nset=NodeRight
*Nset, nset=NodeLeft
*Orientation, name=Ori-1
           1.,           0.,           0.,           0.,           1.,           0.
3, 0.
** Section: SPM
*Solid Section, elset=Set-1, orientation=Ori-1, material=SPM
,
*End Part
**
**
** ASSEMBLY
**
*Assembly, name=Assembly
**
*Instance, name=Part-1-1, part=Part-1
*End Instance
**
*Nset, nset=Set-1, instance=Part-1-1
*Elset, elset=Set-1, instance=Part-1-1
*Nset, nset=backside, instance=Part-1-1, generate
*Elset, elset=backside, instance=Part-1-1, generate
*Nset, nset=Bot, instance=Part-1-1
*Elset, elset=Bot, instance=Part-1-1
*Nset, nset=Top, instance=Part-1-1
*Elset, elset=Top, instance=Part-1-1
*End Assembly
*Amplitude, name=Amp-1, definition=SMOOTH STEP
           0.,           0.,           0.01,           1.
```

```
**
** MATERIALS
**
*include,input=matbase1.inp
**
** BOUNDARY CONDITIONS
**
** Name: Bot Type: Displacement/Rotation
*Boundary
Bot, 1, 1
Bot, 2, 2
Bot, 3, 3
Bot, 4, 4
Bot, 5, 5
Bot, 6, 6
** Name: ThickSym Type: Symmetry/Antisymmetry/Encastre
*Boundary
backside, ZSYMM
** Name: Top Type: Displacement/Rotation
*Boundary
Top, 2, 2
Top, 3, 3
Top, 4, 4
Top, 5, 5
Top, 6, 6
** Name: WidthSym Type: Symmetry/Antisymmetry/Encastre
*Boundary
Set-1, YSYMM
** -----
**
** STEP: Step-1
**
*Step, name=Step-1, nlgeom=NO
*Dynamic, Explicit
, 0.1
*Bulk Viscosity
0.06, 1.2
**
** BOUNDARY CONDITIONS
**
** Name: BC-5 Type: Velocity/Angular velocity
*Boundary, amplitude=Amp-1, type=VELOCITY
Top, 1, 1, 8.
**
** OUTPUT REQUESTS
```

```
**
*Restart, write, number interval=1, time marks=NO
**
** FIELD OUTPUT: F-Output-1
**
*Output, field, number interval=150
*Node Output
A, RF, U, V
*Element Output, directions=YES
LE, PE, PEEQ, PEEQAVG, PEAVG, S, SDV, STATUS, SVAVG
**
** HISTORY OUTPUT: H-Output-1
**
*Output, history, variable=PRESELECT
**
** HISTORY OUTPUT: H-Output-4
**
*Output, history, time interval=0.0001
*Node Output, nset=Bot
RF1,
**
** HISTORY OUTPUT: H-Output-2
**
*Node Output, nset=Part-1-1.NodeLeft
U1,
**
** HISTORY OUTPUT: H-Output-3
**
*Node Output, nset=Part-1-1.NodeRight
U1,
*End Step
```